

**RAI: Volume 3, Chapter 2.2.1.3.3, First Set, Number 1:**

Provide the following additional technical bases to demonstrate that measured pore-water compositions can be used in SAR Section 2.3.5.3 to adequately represent the range of compositions in the natural system and can be used to determine the initial water compositions for the near-field chemistry model:

- (a) An explanation for why the sample set used in selecting the starting waters for the near-field chemistry model is representative of the spatial and compositional ranges of waters associated with (1) fracture flow paths and (2) matrix flow paths. Discuss whether the sample set can be used throughout the entire repository.
- (b) Support for the range of initial water compositions for conservative anions, such as chloride ( $\text{Cl}^-$ ) and nitrate ( $\text{NO}_3^-$ ) that are important to corrosion.
- (c) The locations for all 125 pore-water compositions available for the TSW (SNL 2007, Section 6.6). Provide the locations in XYZ space in an electronic format that can be displayed in the DOE Geologic Framework Model. In addition, identify the 90 pore-water compositions that were considered in the screening process (described in SAR Section 2.3.5.3.2.2.1) and the 34 complete compositional analyses of pore waters that were considered in the selection of four initial pore-water inputs to the near-field chemistry model.
- (d) An explanation of uncertainty and its propagation in the near-field chemistry model and performance assessment model. Also address the likely process-level causes for the bimodal distribution of the 34 sample compositions that passed the quality screening criteria (SAR Figure 2.3.5-9).

**Basis:** SAR Section 2.3.5.3.3.2.1 (p. 2.3.5.57) identifies the following key assumption that is built into the near-field chemistry model: “Measured Pore-Water Compositions Adequately Represent the Actual Range of Initial Water Compositions in the Natural System.”

The technical bases used to support the above assumption do not clearly identify the spatial and chemical variability in the natural system as represented by the measured pore-water compositions considered as inputs to the near-field chemistry model (e.g., the chemical similarities in bulk rock analyses do not explicitly consider anions the DOE identifies as important to drip shield or waste package corrosion). The requested information is needed for NRC review of the adequacy of parameter values used in the near-field chemistry model.

## 1. RESPONSE

In this response, each of the points in this RAI is addressed in order. First, in response to Item (a), Section 1.1 provides the basis for concluding that the starting waters for the near-field chemistry (NFC) model are adequate to represent both fracture and matrix waters; this response largely relies on a more complete discussion of flow in the unsaturated zone presented in the response to RAI: 3.2.2.1.3.3-006. It is also concluded that starting waters are applicable throughout the repository, because of compositional homogeneity in the TSw and general overall lithologic similarities in overlying units. Section 1.2 addresses Item (b) by clarifying the implementation of the uncertainty in chloride and nitrate concentrations and chloride-to-nitrate ratios in the NFC model and seepage evaporation abstraction, providing the range of the values used in the models, and showing that it captures the observed range in the 34 pore waters selected for use in the models. It is also shown that these values cover the range likely to be observed throughout the repository footprint. For Item (c), Section 1.3 discusses the available pore-water analyses and points to a thorough discussion of the pore-water screening analysis presented in the response to RAI: 3.2.2.1.3.3-003. Also, tables containing all pore-water compositions and locations (XYZ), with respect to the Nevada State Plane, are provided in Appendix A. An electronic version of the sampling locations, suitable for use in Earthvision Version 7.5.3, is included as Enclosure 7 to the transmittal letter and reproduced in Appendix B of this response. In response to Item (d), Section 1.4 summarizes an existing discussion in *Engineered Barrier System: Physical and Chemical Environment* (SNL 2007a, Section 6.6), describing how uncertainty in pore-water compositions is propagated through the NFC model and how the model fits into the generation of abstractions developed for use in the total system performance assessment model for the license application (TSPA-LA). As discussed in Section 1.5, process-level causes for the observed bimodal distribution in pore-water composition may include variations in interaction times between percolating water and the host rock above the repository.

### 1.1 REPRESENTATIVENESS OF THE NFC MODEL STARTING WATERS

The set of 125 water analyses from the TSw were initially considered in the NFC model. As noted in *Engineered Barrier System: Physical and Chemical Environment* (SNL 2007a, Section 6.6), 35 of these waters were screened from consideration for several reasons, including being incomplete or thermally perturbed or coming from parts of the unit other than those comprising the welded devitrified rhyolite which is the repository host rock. (Note that TSw waters collected from Drift Scale Test boreholes were not evaluated, because they were collected at elevated temperatures and were in almost all cases heavily diluted by condensation processes (SNL 2007a, Section 7.1.4).) The remaining 90 water analyses were sufficiently complete to be considered for use in the model, and were taken from the four repository host units under nominally ambient conditions. A screening process was developed to evaluate sample analysis quality and to screen waters that were affected by microbial activity during core storage. The screening process is described in detail in the response to RAI: 3.2.2.1.3.3-003. The final result of the screening was that 34 water compositions that were determined to be representative of *in situ* conditions at the locations where they were collected.

Justification for assuming that these 34 pore-water analyses are sufficient to represent waters in fracture and matrix flow pathways is provided in the responses to RAI: 3.2.2.1.3.3-006 and RAI: 3.2.2.1.3.3-007. At low percolation flux values (i.e., present-day climate) the fracture and matrix waters are in equilibrium, or near-equilibrium, as demonstrated from interpretation of strontium isotopes in recent fracture-lining calcite. This is part of the basis for the use of matrix pore-water compositions to represent inflowing fracture waters in the NFC model (see the responses to RAI: 3.2.2.1.3.3-006 and RAI: 3.2.2.1.3.3-007). For much higher percolation fluxes possible for future climates, chemical disequilibrium between fracture and matrix waters may occur, but the plug-flow approach implemented in the NFC model is still a valid representation of the residence time because it has been calibrated to the results of the transport simulations that explicitly model matrix and fracture flow. It is likely that both fracture and matrix waters under higher-rainfall future conditions would be more dilute than present-day waters, and may have other chemical differences as well. However, it is assumed that the existing set of matrix pore waters can be used to reasonably bound in-drift water compositions, for two reasons. First, because the ultimate use of these waters is for predicting in-drift chemistry, the relative concentration of the starting waters is of little importance. Even in the long-term, it is the relative humidity in the drift that controls the degree of dilution or concentration that occurs; for instance, even at 1,000,000 years, predicted water concentrations vary by more than two orders of magnitude (see the response to RAI: 3.2.2.1.3.3-017), due to small variations in predicted in-drift relative humidity. Second, the four sets of pore waters represent the three commonly occurring natural water types (SNL 2007a, Section 6.3.3.1). Group 1 waters are carbonate-type waters, evolving into basic Na–K–CO<sub>3</sub>-rich brines (Cl–NO<sub>3</sub>-rich at high degrees of evaporation); Group 2 and Group 3 waters are calcium-chloride-type waters, evolving into acidic calcium- and magnesium-rich chloride and chloride–nitrate brines, respectively; and Group 4 waters evolve into neutral pH Na–K–Cl–NO<sub>3</sub>–SO<sub>4</sub> brines, which are best described with respect to the behavior of calcium as being sulfate-type waters (SNL 2007a, Section 6.13.5.2). Hence, the general evaporative behavior of natural waters is captured using the existing four representative water groups.

These pore waters are assumed to be applicable throughout the repository for several additional reasons. First, the general lithologies of units overlying the repository are similar within the repository footprint, although thicknesses may vary somewhat. Pore waters traveling downward through overlying rocks and through the upper parts of the TSw will be conditioned by the same water–rock reactions, although to different degrees depending upon the rate of percolation. Hence, although geographic distribution of pore-water samples was limited, it is reasonable to assume that the sampling was adequate and representative for the repository footprint.

The degree of water–rock reaction is a function of the contact time, which in turn is a function of the rate of flow through the units (percolation flux) and the depth. The effects of variations in percolation flux on the degree of water–rock interaction are the same as those of depth; both slower percolation fluxes and greater depths correspond to longer contact times and, because the four repository units are mineralogically homogeneous, have an equivalent effect with respect to changes in water chemistry. Samples were collected from all four of the repository host units in the TSw (the lower nonlithophysal zone (Ttptln), lower lithophysal zone (Ttptll), middle nonlithophysal zone (Ttptmn), and upper lithophysal zone (Ttptul)) and show evidence of differing amounts of interaction with minerals in the TSw. Since waters throughout the TSw

were sampled and are included in the 34 samples used in the NFC model, it is likely that the waters represent an adequate and appropriate range of water–rock interactions.

## **1.2 REPRESENTATIVENESS OF THE RANGE OF CHLORIDE AND NITRATE CONCENTRATIONS USED IN THE NFC MODEL**

Water–rock interactions affect non-conservative elements, but do not affect the abundances of chloride and nitrate, or the chloride-to-nitrate ratio. These abundances are determined by the concentrations of those elements in rainwater, by evapotranspiration processes at the surface that serve to concentrate chlorine and NO<sub>3</sub> relative to rain water, and by biological processes in the soil that could affect nitrate concentrations. Justification for the ranges of the chloride and nitrate concentrations and ratios used in the NFC model and seepage evaporation abstraction is provided below.

It is unlikely that rainwater falling on different parts of the repository footprint varies significantly in composition, so concentrations of chloride and nitrate in pore waters are largely due to soil and evapotranspiration processes. Evapotranspiration removes water from the soil and leaves behind many dissolved constituents, such as chloride. Microbial processes in the soil (e.g., denitrification) can affect nitrate concentrations. While small rain events that do not lead to significant infiltration will result in build-up of very small amounts of soluble salts in the soil, these salts would be washed into the subsurface during the next large rain event. Even if these solutes travel by “fast pathways” down to the PTn, the lack of fracture flow through this unit serves to homogenize episodic flow (SNL 2007b, Section 6.9), and will homogenize minor fluctuations in percolating water compositions as well. There is no evidence that build-up of large amounts of soluble salts occurs in soils at Yucca Mountain, and perched waters at the base of the TSw, believed to be “fast pathway” waters, are more dilute than most TSw pore waters. Chloride is unaffected by soil processes, and hence, chloride concentrations are a direct measure of the efficiency of evapotranspiration.

With respect to chloride concentrations, support for the representativeness of the 34 selected water compositions is provided by comparison to the other 56 pore waters that were screened out as being affected by microbial activity during core storage. The screened-out waters can be used for this because microbial activity does not affect chloride concentrations. Although these sample populations are not entirely independent (some waters in each group were collected at the same locations), similarity in the two groups would indicate that they are both representative of the same overall population, and provide support that the population is adequately represented. The 56 waters represent more sampling sites than the 34 waters that were screened in, because they include sample sites along more than 2 km of the Enhanced Characterization of the Repository Block Cross-Drift. The chloride concentration range of the screened-in waters bounds that of the screened-out waters, except for two samples, both with chloride concentrations of 180 mg/L (Figure 1). Cumulative distribution functions for the two data sets are provided in Figure 2. The distributions have nearly identical means and standard deviations. When evaluated using the Wilcoxon Rank Sum Test, a p-value of 0.468 (47%) is calculated. This value represents the probability of incorrectly rejecting the hypothesis that the two sample groups represent the same population; the large value (5% is commonly used as a cutoff) does not indicate that the two samples represent the same population, but rather that they are

similar enough that it is not possible to conclude that they do not. Therefore, the screened-out pore-water samples provide additional confidence that the 34 screened-in samples are representative of the range of chloride concentrations at the site.

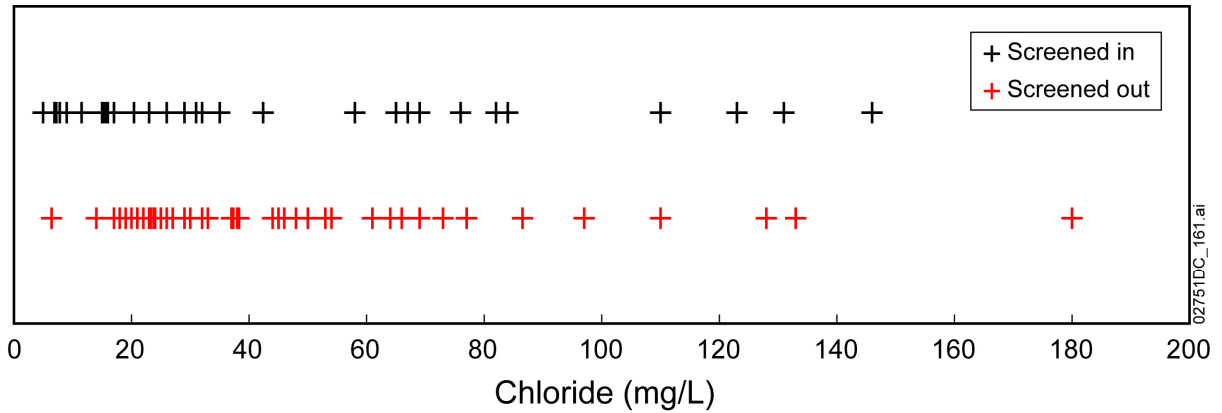


Figure 1. Range of Chloride Concentrations in Screened-in and Screened-out Water Samples

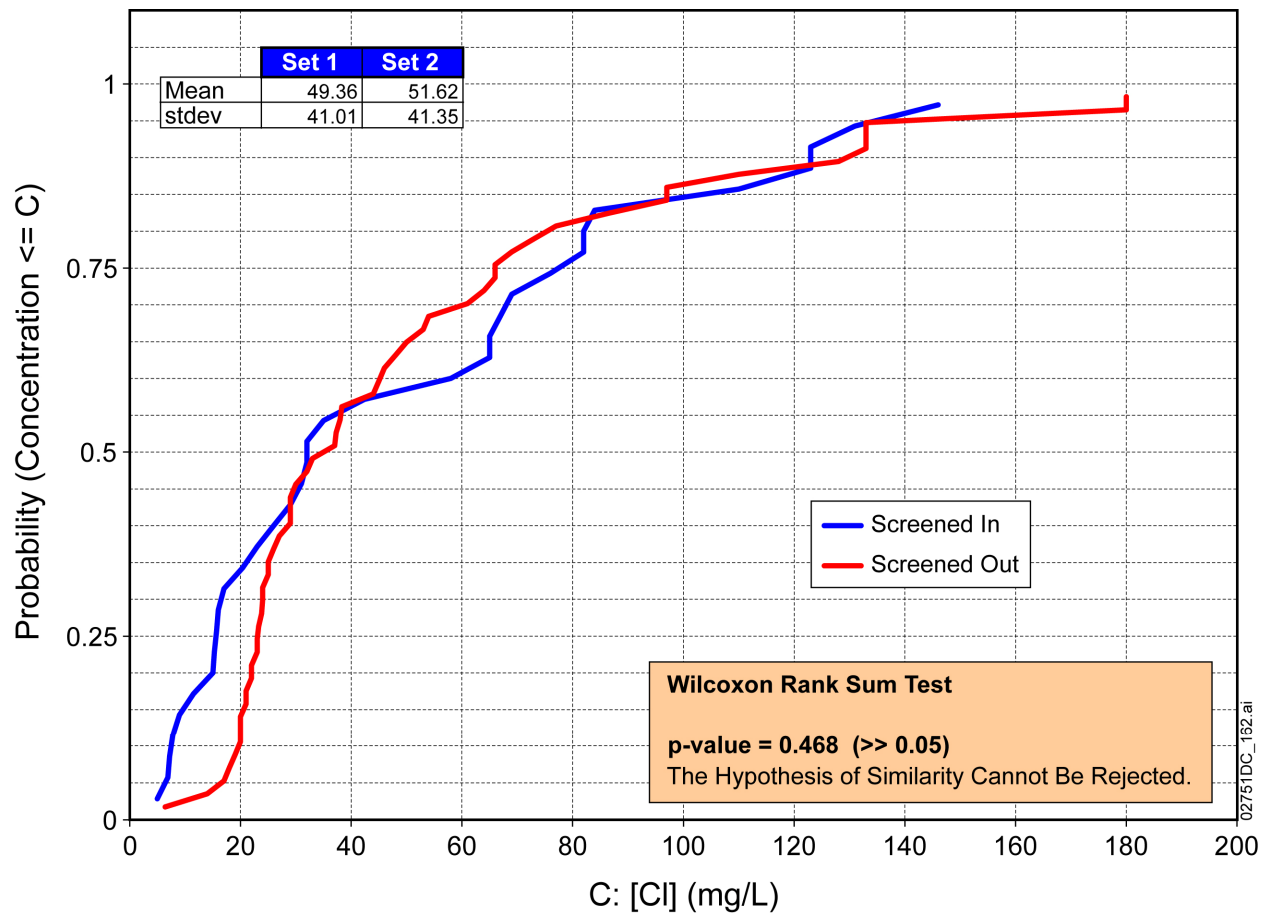
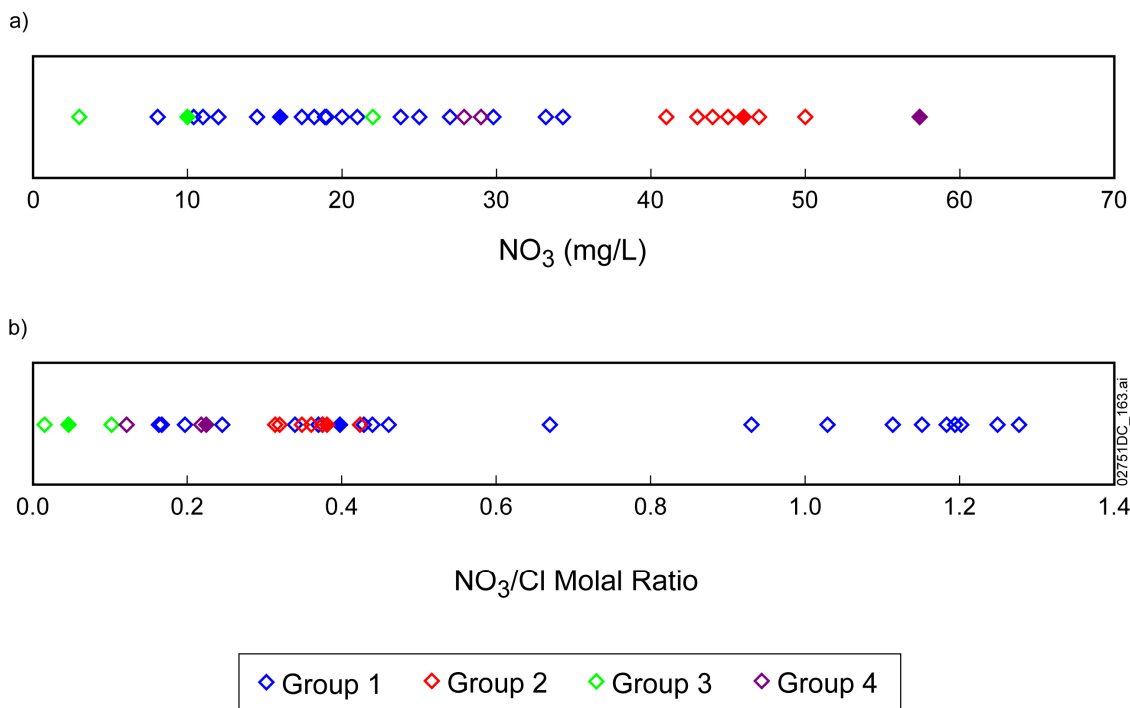


Figure 2. Cumulative Distribution Function Plots of Chloride Concentrations in TSw Pore Waters

Nitrate-to-chloride ratios are high in atmospheric dusts collected at the site, and also in samples collected from near Las Vegas as part of the National Atmospheric Deposition Program/National Trends Network (NADP/NTN) (SNL 2007d, Tables 4.1-8 and 4-3[a]). In pore waters, the ratios are uniformly much lower, indicating that nitrate loss occurs in soils or in the shallow subsurface at the site, probably due to biological processes. Hence, the major processes affecting nitrate concentrations *in situ* are evapotranspiration and biological processes in the shallow subsurface.

The range of nitrate concentrations in the screened-in pore waters is presented in Figure 3(a), and the range of nitrate-to-chloride ratios, in Figure 3(b). Unlike chloride, the screened-out pore-water analyses cannot be used to evaluate the nitrate concentrations in 34 selected waters because most of the screened-out pore waters were affected by microbial activity during core storage, resulting in denitrification (see the response to RAI: 3.2.2.1.3.3-003). The chloride data suggest that the effects of varying evapotranspiration are captured in the range of waters used. The Yucca Mountain soils are relatively thin and vegetation sparse or absent, contributing to the measured unsaturated zone gases containing atmospheric levels of oxygen. Consequently, it is unlikely that any area exists within the repository foot print where soil conditions are reducing and complete depletion of nitrate occurs. The absence of strong reducing environments supports the conclusion that the range of nitrate concentrations is representative or at least bounding.



NOTE: (a) NO<sub>3</sub><sup>-</sup> concentrations (b) NO<sub>3</sub><sup>-</sup>/Cl<sup>-</sup> values (filled symbols are the representative water for each group).

Figure 3. Range of Values in Screened-in TSw Pore Waters

Also, within the suite of samples considered for use in the NFC model, a third process, microbial activity during core storage, also affected nitrate concentrations. The screening analysis for microbial activity during core storage (see response to RAI: 3.2.2.1.3.3-003) selected 34 minimally affected waters for use in the model. The screening criteria were chosen to be inclusive, to retain samples that might have been slightly affected in order to ensure that no waters were inappropriately screened out. Hence, it is likely that the range of nitrate-to-chloride ratios in the screened-in waters is bounding, extending lower than the range applicable to *in situ* conditions.

The applicability of the selected suite of pore waters over the entire repository footprint is an assumption in *Engineered Barrier System: Physical and Chemical Environment* (SNL 2007a, Section 5.2.2). Rainwater falling onto the site is unlikely to vary much from location to location, and based on the chloride concentrations, the effects of evapotranspiration are adequately captured. The effects of soil processes on nitrate concentrations and nitrate-to-chloride ratio are less well-constrained, but the suite of screened-in samples includes some with very low nitrate-to-chloride ratios (<0.1), possibly in part due to microbial activity during core storage; the range is likely bounding with respect to pore-water nitrate-to-chloride ratio, and therefore conservative with respect to corrosion of Alloy 22. Moreover, percolating waters across the site encounter the same rock compositions, and undergo the same water-rock reactions, although the unit thicknesses and distance traveled from the surface, and hence the transport time and degree of interaction, may vary across the site. Samples collected from each of the four repository host units, representing a large vertical extent, encompass a wide range of degree of water-rock interaction.

### **1.3 SUMMARY OF PORE WATERS AVAILABLE FOR THE TSW**

A summary of the 125 TSW pore-water analyses considered for use in the NFC model is provided in Appendix A. Table A-1 provides sample locations, and Table A-2 provides pore-water chemistry and storage conditions. This list represents all complete or nearly complete pore-water analyses available from the unit, except for samples associated with the Drift Scale Test, which were known to be heavily modified by condensation and degassing processes. The Drift Scale Test samples were specifically excluded from consideration because the goal of the analysis was to identify the range of pore-water compositions representing ambient conditions. A thorough discussion of the pore water screening analysis is given in the response to RAI: 3.2.2.1.3.3-003.

Additionally, an electronic file containing the pore water sample location information in the form of XYZ coordinates relative to the Nevada State Plane is provided with the transmittal letter for this RAI response (Enclosure 7). This text file, the contents of which are also reproduced in Appendix B, can be read by Earthvision Version 7.5.3, as used in *Geologic Framework Model* (BSC 2004).

#### 1.4 PROPAGATION OF UNCERTAINTY IN STARTING WATER COMPOSITIONS THROUGH THE NFC MODEL AND INTO THE TSPA-LA MODEL

Uncertainty in the 34 initial pore-water compositions is propagated into the NFC model in two ways. First the pore waters were statistically binned into 4 groups on the basis of initial chemistry and predicted chemistry upon evaporation (SNL 2007a, Section 6.6.5). The results of the binning process are illustrated in Figure 4. As discussed previously, Group 1 waters evolve to higher pH, Na–K–CO<sub>3</sub>-rich waters upon evaporation. Groups 2 and 3 waters evolve to lower pH, calcium-rich and carbonate-poor waters; these two groups are distinguished primarily by their NO<sub>3</sub><sup>-</sup> versus Cl<sup>-</sup> concentrations. Group 4 waters evolve to near-neutral pH waters. Following grouping, the representative water for each group was chosen by finding the point nearest to the centroid of each group in the *n*-dimensional space represented by <sup>*n*</sup>/<sub>2</sub> compositional components each at initial and 74% relative humidity conditions. The four representative waters are identified in Table 1.

To explain how these waters are used and how uncertainty in initial water compositions is propagated through to the TSPA-LA model, it is necessary to explain how the NFC model couples with the seepage evaporation abstraction and with the TSPA-LA model (SAR Sections 2.3.5.3.4 and 2.3.5.5.4). This is illustrated in a flow chart in Figure 5. The four waters identified in Table 1 are used as the starting waters in the NFC model. Because TSPA calculations do not use seepage water compositions (representing seepage before it enters the drift) directly, but rather calculate in-drift water compositions, these four starting waters are not used to calculate a time history of seepage compositions. Instead, the four waters are used to parametrically generate a set of seepage water compositions, in the form of EQ3/6 pickup files, at 11 discrete water–rock interaction parameter (WRIP) values (amounts of feldspar dissolved), and at three different temperatures (30°C, 70°C, and 96°C) for use as initial water compositions by the in-drift seepage evaporation abstraction. There are a total of 132 pickup files ( $11 \times 4 \times 3 = 132$ ). The seepage evaporation abstraction in turn generates 396 lookup tables by simulating evaporation of the 132 seepage water compositions at *p*CO<sub>2</sub> values of 10<sup>-2</sup>, 10<sup>-3</sup>, and 10<sup>-4</sup> bars; the temperatures used are the same as those used in the NFC model calculations, except 100°C is used instead of 96°C. The seepage evaporation abstraction lookup tables provide potential in-drift water compositions as a function of relative humidity. Each lookup table is identified by four parameters—the initial group water (4), the WRIP value (11), the temperature (3), and the in-drift *p*CO<sub>2</sub> (3).

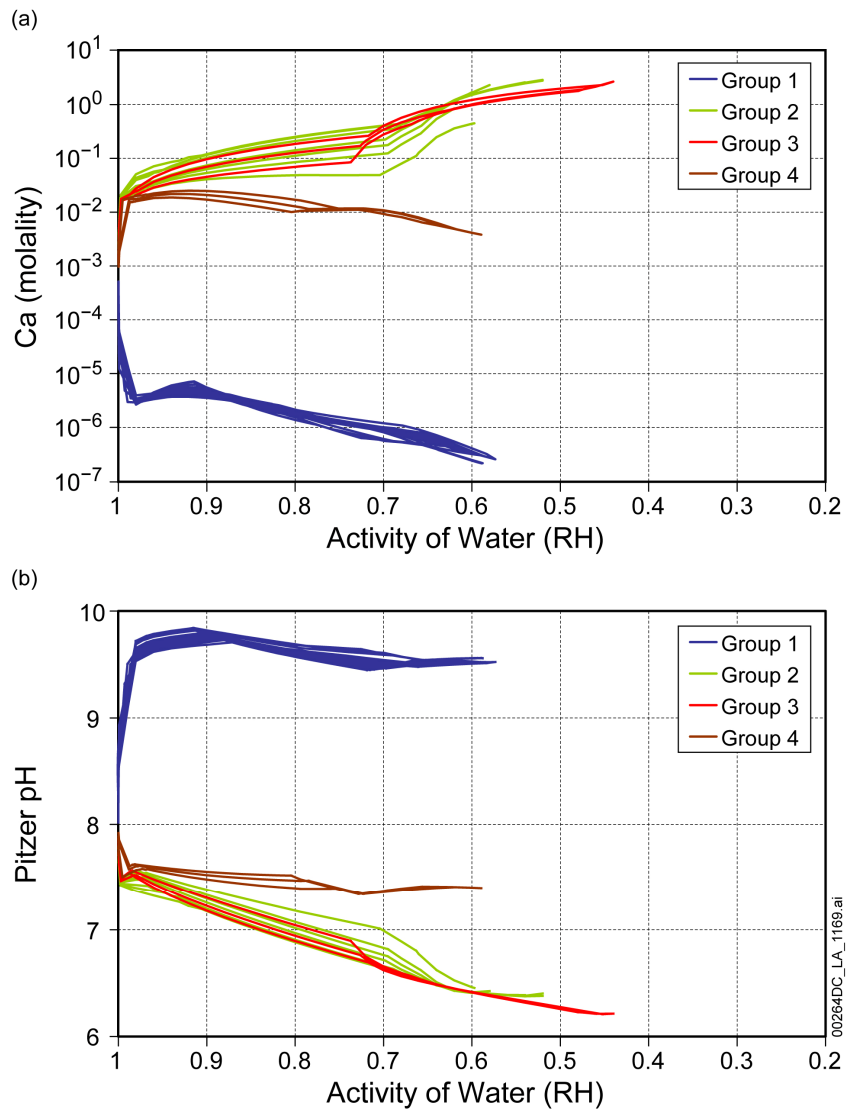


Figure 4. Evaporative Evolution of the 34 TSw Pore Waters Used in the NFC Model ( $p\text{CO}_2 = 10^{-3}$  bars;  $T = 25^\circ\text{C}$ )

Table 1. Representative Waters for Each of the Four Water Groups

Group	# Waters	Representative Water	EQ3/6 filename
1	21	SD-9/1184.7-1184.8/UC	SD9-3
2	7	ESF-THERMALK-017/26.5-26.9/UC	ESFTHER1
3	3	ESF-HD-PERM-3/34.8-35.1/Alcove 5	ESFPERM3
4	3	HD-PERM-3/56.7-57.1/UC	ESFPERM4

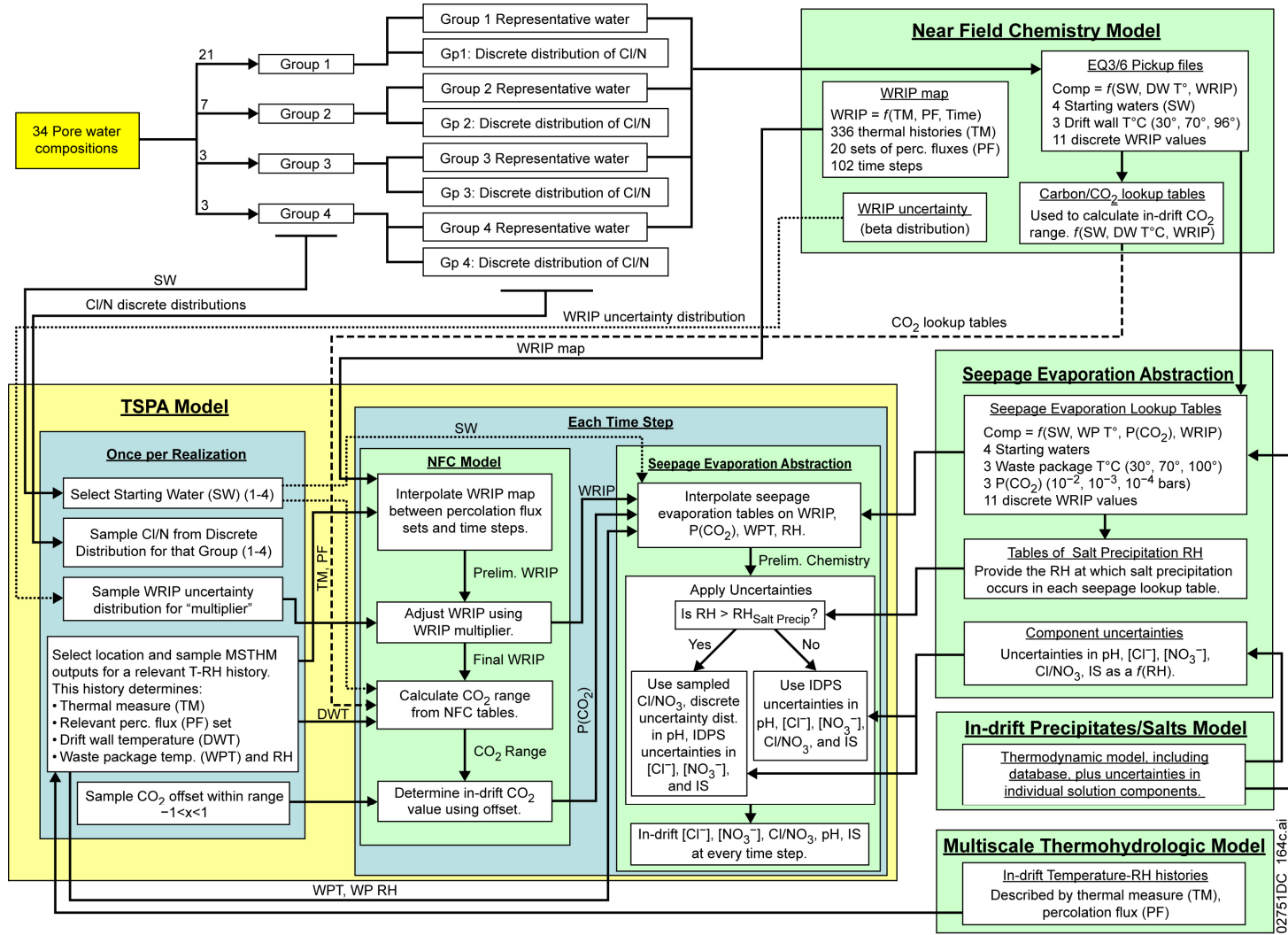


Figure 5. Flow Chart Illustrating How the NFC Model and Seepage Evaporation Abstraction Are Integrated into TSPA

For any given TSPA-LA model realization, one of the four starting waters is randomly selected. Each of the waters is weighted equally (SAR Section 2.3.5.5.4.3), even though the groups contain different numbers of pore-water samples. The TSPA-LA model then selects a sequence of percolation fluxes (four values, representing the present-day, monsoonal, glacial-transition, and post-10,000-year climate scenarios) and a thermal history for a location of interest from the outputs of *Multiscale Thermohydrologic Model* (MSTHM) (SNL 2008). It uses the thermal measure (a metric representing the thermal history) to identify the appropriate set of rows of the WRIP map to use, and the percolation fluxes to identify the appropriate columns at each time step (SAR Section 2.3.5.3.4). A time history of WRIP values is generated, interpolating between columns representing different percolation fluxes as necessary. Uncertainty in the WRIP value, due to uncertainty in the feldspar dissolution rate and water-rock ratio, is sampled once per realization, and implemented as a proportional offset on the values derived from the WRIP map.

To calculate an in-drift water chemistry at each time step, the TSPA-LA model selects a set of bounding seepage evaporation abstraction lookup tables and interpolates between them to determine the value for the component of interest (SAR Section 2.3.5.5.4.3). To select the bounding lookup tables, the TSPA-LA model uses the same sampled starting water; a WRIP value calculated from the WRIP map (adjusted for uncertainty); a group-water-specific  $P(\text{CO}_2)$  sampled from tables provided by the NFC model; and a waste package temperature provided by the MSTHM (SNL 2008). The TSPA-LA model uses an in-drift relative humidity (waste package surface or invert), provided by the MSTHM (SNL 2008), to select the appropriate composition from within the bounding lookup tables, and interpolates on temperature,  $P(\text{CO}_2)$ , and WRIP value to arrive at a single value for each parameter.

Within the NFC model, uncertainty in initial water compositions is only included by the use of four representative waters to represent the 34 screened-in waters. Other uncertainties that are implemented in the NFC model are incorporated into the range used in the WRIP value (SAR Section 2.3.5.3.4). Additional uncertainties are incorporated at the TSPA level through sampling of MSTHM (SNL 2008) thermal histories and percolation flux values (SAR Section 2.3.5.3.2.2.2).

Because histories of in-drift water composition through time are calculated, rather than histories of seepage composition, no uncertainty is attached to the seepage chemistries that are passed to the seepage evaporation abstraction in EQ3/6 pickup files. The uncertainties in the WRIP value are incorporated in the next step, when the TSPA-LA model selects the seepage evaporation abstraction lookup tables to sample. Uncertainties in individual chemical components important to the TSPA analyses are applied to the seepage evaporation abstraction results, and it is at this point that the variability in initial nitrate-to-chloride ratios is added (SAR Section 2.3.5.5.4.3). At relative humidity values above that at which a chloride- or nitrate-containing salt mineral saturates and precipitates, chloride and nitrate display very weak interactions with other species in solution, and, within limits, are interchangeable. So long as the sum of  $[\text{NO}_3^- + \text{Cl}^-]$  is constant, the two individual component concentrations may vary widely. Within the range of nitrate-to-chloride ratios present in any one of the four water groups, it is possible to partition nitrate and chloride according to any nitrate-to-chloride ratio, while holding the sum constant, without having any significant effect on other water components. Therefore, at relative humidity values above that of salt saturation, once the seepage evaporation abstraction lookup tables have

been queried and chloride and nitrate concentrations determined, the value of  $[\text{NO}_3^- + \text{Cl}^-]$  is calculated, and uncertainties from the in-drift precipitates/salts (IDPS) model (SNL 2007c) are applied. Then a value of Cl:N is sampled from a discrete distribution of the pore-water values for that water group (see Figure 3(b)), and  $\text{Cl}^-$  and  $\text{NO}_3^-$  concentrations are back-calculated using the value of  $[\text{NO}_3^- + \text{Cl}^- + \text{uncertainty}]$  and the selected Cl:N ratio (all chlorine is assumed to be present as  $\text{Cl}^-$  and all nitrogen as  $\text{NO}_3^-$ ; this assumption is valid over the pH range predicted to occur, at relative humidity values above salt saturation). The value of Cl:N is sampled by the TSPA-LA model only once per realization, when the starting water group is selected. Below the relative humidity at which salt saturation occurs,  $\text{Cl}^-$  and  $\text{NO}_3^-$  concentrations are taken directly from the seepage evaporation abstraction lookup tables, IDPS uncertainties are applied, and the  $\text{Cl}^-/\text{NO}_3^-$  value is calculated. Therefore, below the relative humidity of salt saturation, only the four representative waters are used in the TSPA-LA model calculations of  $\text{Cl}^-$  and  $\text{NO}_3^-$  concentrations and the  $\text{Cl}^-/\text{NO}_3^-$  ratio. This has no impact with respect to initiation of localized corrosion, because if brine is predicted to contact the waste package at a relative humidity below that of salt saturation, then localized corrosion is always assumed to initiate when the relative humidity later increases above that value (SAR Section 2.3.5.5.4.3). This is because the precipitated salts could potentially be separated from the remaining brine. The salt separation aspects of localized corrosion are discussed in the response to RAI: 3.2.2.1.3.1-2-011.

## 1.5 POSSIBLE CAUSES FOR THE BIMODAL DISTRIBUTION IN SCREENED-IN PORE-WATER COMPOSITIONS

Once the available suite of TSw pore-water samples were screened for microbial activity during core storage, the remaining samples showed a strong bimodal distribution. The screening analysis is described in *Engineered Barrier System: Physical and Chemical Environment* (SNL 2007a, Section 6.6), and additional information, validating the original screening decisions, is provided in the response to RAI: 3.2.2.1.3.3-003. The 34 samples that passed the screening analysis for microbial activity display a bimodal distribution on a Piper diagram. One group of waters is Ca-Cl- $\text{NO}_3$  or Ca-Cl-rich; the other is Na-Cl- $\text{NO}_3$ -rich. The relatively calcium-rich waters correspond to Groups 2, 3, and 4 in Figure 4, while the sodium-rich waters correspond to Group 1. In either group, nitrate concentrations can be either relatively high, with molal concentrations as high as chloride, or much lower. This suggests that the differences are unrelated to microbial modification during core storage, and that the different water types represent *in situ* variations in pore-water composition. They may represent variations in the degree of interaction between the percolating waters and minerals and glass in the geologic section above the repository, because dissolution of alkali feldspar or of rhyolitic glass, followed by precipitation of calcium-containing clays or zeolites, will generally result in depletion of calcium from solution and an increase in sodium and potassium concentrations. The compositional differences do not show a strong correlation with stratigraphic unit in the TSw. However, the degree of water-rock interaction is a function of contact time, which varies both with distance traveled and with percolation flux, so a clear correlation with depth need not exist. Hence, the Group 1 waters may represent a higher degree of water-rock interaction than the Group 2, 3, and 4 waters.

## 2. COMMITMENTS TO NRC

None.

## 3. DESCRIPTION OF PROPOSED LA CHANGE

None.

## 4. REFERENCES

BSC (Bechtel SAIC Company) 2004. *Geologic Framework Model (GFM2000)*. MDL-NBS-GS-000002 REV 02. Las Vegas, Nevada: Bechtel SAIC Company. ACC: DOC.20040827.0008.

SNL (Sandia National Laboratories) 2007a. *Engineered Barrier System: Physical and Chemical Environment*. ANL-EBS-MD-000033 REV 06. Las Vegas, Nevada: Sandia National Laboratories. ACC: DOC.20070907.0003; LLR.20080328.0031.

SNL 2007b. *UZ Flow Models and Submodels*. MDL-NBS-HS-000006 REV 03 AD 01. Las Vegas, Nevada: Sandia National Laboratories. ACC: DOC.20080108.0003; DOC.20080114.0001; LLR.20080414.0007; LLR.20080414.0033; LLR.20080522.0086.

SNL 2007c. *In-Drift Precipitates/Salts Model*. ANL-EBS-MD-000045 REV 03. Las Vegas, Nevada: Sandia National Laboratories. ACC: DOC.20070306.0037; LLR.20080401.0242; DOC.20080707.0001.

SNL 2007d. *Analysis of Dust Deliquescence for FEP Screening*. ANL-EBS-MD-000074 REV 01 AD 01. Las Vegas, Nevada: Sandia National Laboratories. ACC: DOC.20070911.0004; DOC.20070824.0001; DOC.20080109.0005.

SNL 2008. *Multiscale Thermohydrologic Model*. ANL-EBS-MD-000049 REV 03 AD 02. Las Vegas, Nevada: Sandia National Laboratories. ACC: DOC.20080201.0003; LLR.20080403.0162; LLR.20080617.0077.

**APPENDIX A****TSW PORE-WATER LOCATIONS, SCREENING STATUS, AND CHEMISTRY**

In this appendix, the locations of the 125 pore-water samples considered as possible starting waters in the NFC model are provided (Table A-1). The XYZ locations are given relative to the Nevada State Plane and to mean sea level (MSL), in units of “feet” to be consistent with *Geologic Framework Model* (BSC 2004). An electronic file containing the location information and suitable for use in Earthvision Version 7.5.3 will be included as Enclosure 7 to the transmittal letter; the contents of that file are also reproduced in Appendix B of this response.

Also provided (Table A-2) is the chemistry of the pore waters and their screening status with respect to the pore-water screening analysis for microbial activity during core storage. The screening analysis is discussed in detail in the response to RAI: 3.2.2.1.3.3-003, and additional information (e.g., core storage conditions) is provided there.

Table A-1. Locations for TSw Pore-Water Samples

Sample Name	Location, Relative to the Nevada State Plane		Elevation Relative to MSL, (Feet (Z))
	Easting, (Feet (X))	Northing, (Feet (Y))	
ECRB-DS3-1616/7.5-7.7/UC	559920.8	765346.8	3,629.4
ECRB-DS3-1616/7.7-7.9/UC	559920.8	765346.8	3,629.4
ECRB-DS3-1616/7.9-8.0/UC	559920.8	765346.8	3,629.4
ECRB-DS3-1616/8.0-8.1/UC	559920.8	765346.8	3,629.4
ECRB-DS3-1616/9.6-9.8/UC	559920.8	765346.8	3,629.4
ECRB-DS3-1616/9.8-10.1/UC	559920.8	765346.8	3,629.4
ECRB-DS3-1616/10.1-10.4/UC	559920.8	765346.8	3,629.4
ECRB-DS3-1616/10.6-11.0/UC	559920.8	765346.8	3,629.4
ECRB-DS3-1616/12.5-12.7/UC	559920.8	765346.8	3,629.4
ECRB-DS3-1616/12.7-13.3/UC	559920.8	765346.8	3,629.4
ESF-HD-PERM-1	562501.6	767933.6	3,461.7
ESF-HD-PERM-2	562500.6	767930.8	3,464.2
ESF-HD-PERM-3	562498.8	767924.9	3,461.8
ESF-THERMALK-017/16.6-17.2/UC	562184.8	756735.6	3,687.5
ESF-THERMALK-017/22.3-22.9/UC	562184.8	756735.6	3,687.5
ESF-THERMALK-017/22.9-23.0/UC	562184.8	756735.6	3,687.5
ESF-THERMALK-017/26.3-26.5/UC	562184.8	756735.6	3,687.5
ESF-THERMALK-017/26.5-26.9/UC	562184.8	756735.6	3,687.5
ESF-THERMALK-019/19.2-19.5/UC	562186.7	756735.6	3,686.8
ESF-THERMALK-019/19.5-19.7/UC	562186.7	756735.6	3,686.8
HD-PERM-3/22.4-23.0/UC	562498.8	767924.9	3,461.8
HD-PERM-3/56.7-57.1/UC	562498.8	767924.9	3,461.8
NRG-7/7A/839.3-839.8/UC	562984.0	768880.1	3,367.9

Table A-1. Locations for TSw Pore-Water Samples (Continued)

Sample Name	Location, Relative to the Nevada State Plane		Elevation Relative to MSL (feet (Z))
	Easting (feet (X))	Northing (feet (Y))	
SD-9/669.1-669.2/UC	561818.0	767998.5	3,603.5
SD-9/991.7-992.1/UC	561818.0	767998.5	3,280.9
SD-9/1060.1-1060.5/UC	561818.0	767998.5	3,212.5
SD-9/1119.7-1119.9/UC	561818.0	767998.5	3,152.9
SD-9/1184.7-1184.8/UC	561818.0	767998.5	3,087.9
SD-9/1184.8-1185.0/UC	561818.0	767998.5	3,087.8
SD-9/1185.0-1185.3/UC1	561818.0	767998.5	3,087.6
SD-9/1234.9-1235.1/UC	561818.0	767998.5	3,037.7
SD-9/1276.5-1276.8/UC	561818.0	767998.5	2,996.1
SD-9/1276.8-1277.0/UC	561818.0	767998.5	2,995.8
SD-9/1303.4-1303.9/UC	561818.0	767998.5	2,969.2
ECRB-DS2-1613/13.2-13.4/UC	559927.8	765353.0	3,635.9
ECRB-DS2-1613/18.6-18.9/UC	559927.8	765353.0	3,635.9
ECRB-DS3-1616/7.1-7.5/UC	559920.8	765346.8	3,629.4
ECRB-DS3-1616/8.7-8.9/UC	559920.8	765346.8	3,629.4
ECRB-DS3-1616/10.4-10.6/UC	559920.8	765346.8	3,629.4
ECRB-DS3-1616/11.5-12.5/UC	559920.8	765346.8	3,629.4
ECRB-SYS-CS400/3.8-4.3/UC	562935.6	767956.0	3,573.5
ECRB-SYS-CS400/5.6-6.2/UC	562935.6	767956.0	3,573.5
ECRB-SYS-CS450/5.3-6.0/UC	562812.7	767849.3	3,576.5
ECRB-SYS-CS500/12.0-16.7/UC	562689.3	767742.1	3,579.7
ECRB-SYS-CS600/3.6-4.0/UC	562439.7	767525.3	3,585.9
ECRB-SYS-CS700/5.5-5.8/UC	562191.7	767309.8	3,591.7
ECRB-SYS-CS750/6.2-6.5/UC	562071.5	767205.0	3,594.6
ECRB-SYS-CS800/4.9-5.6/UC	561946.5	767096.5	3,597.4
ECRB-SYS-CS850 5.1-5.6/UC	561823.0	766989.2	3,599.8
ECRB-SYS-CS900/2.8-3.0/UC	561696.8	766879.5	3,602.5
ECRB-SYS-CS900/3.0-3.2/UC	561696.8	766879.5	3,602.5
ECRB-SYS-CS900/3.5-4.1/UC	561696.8	766879.5	3,602.5
ECRB-SYS-CS900/5.4-5.9/UC	561696.8	766879.5	3,602.5
ECRB-SYS-CS950/4.8-5.5/UC	561574.9	766773.5	3,604.6
ECRB-SYS-CS950/5.2-5.3/UC	561574.9	766773.5	3,604.6
ECRB-SYS-CS1000/10.9-11.1/UC	561450.6	766665.7	3,607.2
ECRB-SYS-CS1000/11.1-11.6/UC	561450.6	766665.7	3,607.2
ECRB-SYS-CS1000/12.9-14.0/UC	561450.6	766665.7	3,607.2
ECRB-SYS-CS1000/15.6-15.8/UC	561450.6	766665.7	3,607.2
ECRB-SYS-CS1000/5.4-6.1/UC	561450.6	766665.7	3,607.2
ECRB-SYS-CS1000/7.3-7.7/UC	561450.6	766665.7	3,607.2
ECRB-SYS-CS1100/3.7-3.8/UC	561202.7	766449.9	3,612.1
ECRB-SYS-CS1150/3.2-3.8/UC	561079.4	766342.7	3,614.3

Table A-1. Locations for TSw Pore-Water Samples (Continued)

Sample Name	Location, Relative to the Nevada State Plane		Elevation Relative to MSL (feet (Z))
	Easting (feet (X))	Northing (feet (Y))	
ECRB-SYS-CS1250/3.4-4.0/UC	560831.5	766127.2	3,619.5
ECRB-SYS-CS1250/5.0-5.7/UC	560831.5	766127.2	3,619.5
ECRB-SYS-CS1500/10.0-12.1/UC	560216.0	765592.2	3,631.4
ECRB-SYS-CS2000/16.3-16.5/UC	558977.6	764515.5	3,647.7
ECRB-SYS-CS2000/16.5-21.1/UC	558977.6	764515.5	3,647.7
ECRB-SYS-CS2000/3.3-3.8/UC	558977.6	764515.5	3,647.7
ECRB-SYS-CS2000/3.95-4.1/UC	558977.6	764515.5	3,647.7
ECRB-SYS-CS2150/5.5-6.1/UC	558606.7	764193.0	3,652.4
ECRB-SYS-CS2250/5.2-5.6/UC	558356.3	763975.4	3,655.5
ECRB-SYS-CS2300/4.3-4.9/UC	558232.3	763867.8	3,656.8
ECRB-SYS-CS2300/6.1-6.7/UC	558232.3	763867.8	3,656.8
ECRB-SYS-CS2350/5.0-5.7/UC	558105.0	763763.5	3,658.5
ESF-SAD-GTB#1/119.4-120.0/UC	562159.9	760597.1	3,623.8
ESF-SAD-GTB#1/126.1-126.4/UC	562159.9	760597.1	3,623.8
ESF-SAD-GTB#1/194.2-195.2/UC	562159.9	760597.1	3,623.8
ESF-SAD-GTB#1/195.4-196.7/UC	562159.9	760597.1	3,623.8
ESF-SAD-GTB#1/199.0-199.3/UC	562159.9	760597.1	3,623.8
HD-PERM-2/19.3-19.7/UC	562500.6	767930.8	3,464.2
HD-PERM-2/34.5-34.9/UC	562500.6	767930.8	3,464.2
HD-PERM-2/61.7-62.3/UC	562500.6	767930.8	3,464.2
SD-9/670.5-670.6/UC	561818.0	767998.5	3,602.1
SD-9/990.4-991.7/UC	561818.0	767998.5	3,282.2
SD-9/1184.0-1184.2/UC	561818.0	767998.5	3,088.6
SD-9/1236.4-1236.8/UC	561818.0	767998.5	3,036.2
SD-9/1275.6-1276.0/UC	561818.0	767998.5	2,997.0
SD-9/1330.4-1330.7/UC	561818.0	767998.5	2,942.2
SD-12/1053.7-1054.1 UC-1	561605.6	761956.6	3,289.1
ESF-HD-ChemSamp-1/26.1-26.9/UC	562365.5	767846.3	3,472.0
ESF-HD-ChemSamp-1/28.8-29.7/UC	562365.5	767846.3	3,472.0
ESF-HD-ChemSamp-1/34.6-35.4/UC	562365.5	767846.3	3,472.0
ESF-HD-ChemSamp-1/37.1-37.2/UC	562365.5	767846.3	3,472.0
ESF-HD-ChemSamp-3/104.6-105.3/UC	562363.3	767842.7	3,462.8
ESF-HD-ChemSamp-3/108.4-109.0/UC	562363.3	767842.7	3,462.8
ESF-HD-ChemSamp-3/111.8-112.0/UC	562363.3	767842.7	3,462.8
ESF-HD-ChemSamp-3/113.1-113.8/UC	562363.3	767842.7	3,462.8
ESF-HD-ChemSamp-3/115.0-115.6/UC	562363.3	767842.7	3,462.8
ESF-HD-ChemSamp-3/127.1-128.0/UC	562363.3	767842.7	3,462.8
ESF-HD-ChemSamp-3/33.9-34.4/UC	562363.3	767842.7	3,462.8
ESF-HD-ChemSamp-3/34.4-34.5/UC	562363.3	767842.7	3,462.8
ESF-HD-ChemSamp-3/36.5-37.5/UC	562363.3	767842.7	3,462.8

Table A-1. Locations for TSw Pore-Water Samples (Continued)

Sample Name	Location, Relative to the Nevada State Plane		Elevation Relative to MSL (feet (Z))
	Easting (feet (X))	Northing (feet (Y))	
ESF-HD-ChemSamp-3/38.2-39.1/UC	562363.3	767842.7	3,462.8
ESF-HD-ChemSamp-3/42.3-42.8/UC	562363.3	767842.7	3,462.8
ESF-HD-ChemSamp-3/46.0-46.3/UC	562363.3	767842.7	3,462.8
ESF-HD-ChemSamp-3/46.3-46.9/UC	562363.3	767842.7	3,462.8
SD-6/1509.9 – 1510.3/UC1	558607.7	762421.4	3,395.4
SD-9 /669.8-669.9/UC1	561818.0	767998.5	3,602.8
SD-9/ 669.7-669.8/UC1	561818.0	767998.5	3,602.9
SD-9/1095.6-1096.0/UC	561818.0	767998.5	3,177.0
SD-9/669.0-669.1/UC1	561818.0	767998.5	3,603.6
UZ14-1258.5-1258.8/UP-1	560141.6	771309.8	3,166.9
UZ14-1277.4-1277.7/UP-1	560141.6	771309.8	3,148.0
UZ14-1277.7-1278.0/UP-1	560141.6	771309.8	3,147.7
UZ14A/384.6	560141.6	771309.8	4,040.8
UZ14A2/384.6	560141.6	771309.8	4,040.8
UZ14B/387.68	560141.6	771309.8	4,037.7
UZ14C/390.75	560141.6	771309.8	4,034.7
UZ14D/390.75	560141.6	771309.8	4,034.7
UZ14PT-1/390.75	560141.6	771309.8	4,034.7
UZ14PT-2/390.75	560141.6	771309.8	4,034.7
UZ14PT-4/390.75	560141.6	771309.8	4,034.7
UZ16-1166.19-1166.47/UP-1	564857.5	760535.1	2,834.3
UZ16-952.6-952.9/UP-1	564857.5	760535.1	3,047.9

Table A-2. Screening Status, Chemistry, and Core Storage Conditions for TSw Pore Waters

Screening Status	Sample Name	Storage Condition	Lithologic Unit	Group # (Rep. Water <sup>a</sup> )	pH	Na (mg/L)	K (mg/L)	Mg (mg/L)	Ca (mg/L)	Cl (mg/L)	SO <sub>4</sub> (mg/L)	HCO <sub>3</sub> (mg/L)	NO <sub>3</sub> (mg/L)	F (mg/L)	Br (mg/L)	SiO <sub>2</sub> (mg/L)	Mn (ug/L)	Sr (ug/L)	Sum of Cations <sup>b</sup>	Sum of Anions <sup>c</sup>	Charge Balance % <sup>d</sup>
In	ECRB-DS3-1616/7.5-7.7/UC	Aluminum Foil, Lexan Tube, Protecore <sup>2</sup>	Tptpul	1	—	52.9	5.9	0.81	28.7	15.7	25.3	107	34.3	1.66	0.2	55	7.1	183	3.95	3.36	8.08
In	ECRB-DS3-1616/7.7-7.9/UC	Aluminum Foil, Lexan Tube, Protecore <sup>2</sup>	Tptpul	1	—	50.9	7.27	0.72	25.4	15.3	19.5	107	29.8	1.46	<0.03	51	9.9	162	3.73	3.15	8.46
In	ECRB-DS3-1616/7.9-8.0/UC	Aluminum Foil, Lexan Tube, Protecore <sup>2</sup>	Tptpul	1	—	36.5	4.1	0.35	16.7	7.79	10.5	82	17.4	1.16	0.1	52	19	107	2.56	2.12	9.26
In	ECRB-DS3-1616/8.0-8.1/UC	Aluminum Foil, Lexan Tube, Protecore <sup>2</sup>	Tptpul	1	—	46.9	5.63	0.59	23.4	11.5	15.4	115	23.8	1.59	<0.03	58	5.7	158	3.40	3.00	6.35
In	ECRB-DS3-1616/9.6-9.8/UC	Aluminum Foil, Lexan Tube, Protecore <sup>2</sup>	Tptpul	1	—	36.8	6.06	0.73	16.5	6.89	5.29	113	8.07	1.38	<0.03	42	1.6	65	2.64	2.36	5.63
In	ECRB-DS3-1616/9.8-10.1/UC	Aluminum Foil, Lexan Tube, Protecore <sup>2</sup>	Tptpul	1	—	38	5.77	0.76	20.7	4.98	8.84	149	10.4	1.35	<0.06	46	3.3	120	2.90	3.01	-1.80
In	ECRB-DS3-1616/10.1-10.4/UC	Aluminum Foil, Lexan Tube, Protecore <sup>2</sup>	Tptpul	1	—	39.8	6.03	0.91	20.1	7.2	9.48	128	14.5	1.51	<0.03	39	12	90	2.97	2.81	2.66
In	ECRB-DS3-1616/10.6-11.0/UC	Aluminum Foil, Lexan Tube, Protecore <sup>2</sup>	Tptpul	1	—	61	7.68	1.44	34.1	20.4	22.3	142	33.2	2.32	<0.05	46	14	211	4.67	4.02	7.48
In	ECRB-DS3-1616/12.5-12.7/UC	Aluminum Foil, Lexan Tube, Protecore <sup>2</sup>	Tptpul	1	—	32.5	4.21	0.91	23.5	8.99	13.2	123	18.9	1.15	<0.06	38	14	119	2.77	2.91	-2.43
In	ECRB-DS3-1616/12.7-13.3/UC	Aluminum Foil, Lexan Tube, Protecore <sup>2</sup>	Tptpul	1	—	51.4	6.81	1.05	28.8	15	17.8	166	27	1.86	<0.06	44	7.9	166	3.94	4.05	-1.38
In	ESF-HD-PERM-1	Lexan Tube, Protecore	Tptpmn	3	7.79	61	6	25.7	98	123	124	—	22	0.36	0.6	79	—	1400	—	—	—
In	ESF-HD-PERM-2	Lexan Tube, Protecore	Tptpmn	3	8.32	61	7	16.6	106	110	111	—	3	0.96	0.76	66	—	1000	—	—	—
In	ESF-HD-PERM-3	Lexan Tube, Protecore	Tptpmn	3 <sup>a</sup>	8.31	62	9	17.4	97	123	120	—	10	0.76	1.2	75	—	1100	—	—	—
In	ESF-THERMALK-017/16.6-17.2/UC	Aluminum Foil, Lexan Tube, Protecore <sup>1</sup>	Tptpul	2	—	51	14.2	9.8	73	82	105	104	45	1.3	0.33	63	15	451	7.04	7.00	0.31
In	ESF-THERMALK-017/22.3-22.9/UC	Aluminum Foil, Lexan Tube, Protecore <sup>1</sup>	Tptpul	2	—	48	14.1	7.8	60	65	86	95	41	1.5	0.4	51	14	335	6.09	5.92	1.42

Table A-2. Screening Status, Chemistry, and Core Storage Conditions for TSw Pore Waters (Continued)

Screening Status	Sample Name	Storage Condition	Lithophysal Unit	Group # (Rep. Water <sup>a</sup> )	pH	Na (mg/L)	K (mg/L)	Mg (mg/L)	Ca (mg/L)	Cl (mg/L)	SO <sub>4</sub> (mg/L)	HCO <sub>3</sub> (mg/L)	NO <sub>3</sub> (mg/L)	F (mg/L)	Br (mg/L)	SiO <sub>2</sub> (mg/L)	Mn (ug/L)	Sr (ug/L)	Sum of Cations <sup>b</sup>	Sum of Anions <sup>c</sup>	Charge Balance %
In	ESF-THERMALK-017/22.9-23.0/UC	Aluminum Foil, Lexan Tube, Protecore <sup>1</sup>	Tptpul	2	7.9	37	14.5	9.9	72	69	94	116	46	1.1	0.35	55	14	429	6.40	6.60	-1.59
In	ESF-THERMALK-017/26.3-26.5/UC	Aluminum Foil, Lexan Tube, Protecore <sup>1</sup>	Tptpul	2	—	42	13.6	7.6	58	58	76	150	43	1.4	<0.10	58		395	5.70	6.44	-6.09
In	ESF-THERMALK-017/26.5-26.9/UC	Aluminum Foil, Lexan Tube, Protecore <sup>1</sup>	Tptpul	2 <sup>a</sup>	7.7	45	14.4	7.9	62	67	82	126	44	1.4	0.33	52	12	358	6.08	6.45	-2.93
In	ESF-THERMALK-019/19.2-19.5/UC	Aluminum Foil, Lexan Tube, Protecore <sup>1</sup>	Tptpul	2	—	47	13.7	9.0	69	84	80	104	47	0.67	<0.19	62		405	6.59	6.53	0.42
In	ESF-THERMALK-019/19.5-19.7/UC	Aluminum Foil, Lexan Tube, Protecore <sup>1</sup>	Tptpul	2	—	44	13.2	9.1	71	82	82	124	50	0.60	0.30	59	14	379	6.55	6.89	-2.52
In	HD-PERM-3/22.4-23.0/UC	Lexan Tube, Protecore	Tptpmn	4	—	103	14.6	17.4	48.7	131	123	120	27.9	1.6	—	—	—	—	8.72	8.76	-0.23
In	HD-PERM-3/56.7-57.1/UC	Lexan Tube, Protecore	Tptpmn	4 <sup>a</sup>	—	123	13.8	16.7	59.9	146	126	149	57.4	1.3	—	—	—	—	10.07	10.18	-0.54
In	NRG-7/7A/839.3-839.8/UC	Saran Wrap, Lexan Tube, Protecore	Tptpmn	1	7.9	67	6.9	1.6	19	31	24	151	25	2.8	0.1	41	17	410	4.18	4.40	-2.56
In	SD-9/669.1-669.2/UC	Saran Wrap, Lexan Tube, Protecore	Tptpul	4	—	61	6.3	6.9	66	76	75	136	29	1.2	<0.10	49	17	440	6.69	6.46	1.68
In	SD-9/991.7-992.1/UC	Lexan Tube, Protecore	Tptpll	1	7.9	61	5.4	0.60	27	26	13	—	20	3.3	0.10	55	14	220	—	—	—
In	SD-9/1060.1-1060.5/UC	Lexan Tube, Protecore	Tptpll	1	7.6	68	8.8	<0.25	21	32	15	140	21	1.5	<0.16	50	17	185	4.24	3.93	3.77
In	SD-9/1119.7-1119.9/UC	Lexan Tube, Protecore	Tptpll	1	7.7	81	12.8	<0.6	34	32	24	193	19	1.2	<0.18	45	12	281	5.55	4.93	5.90
In	SD-9/1184.7-1184.8/UC	Lexan Tube, Protecore	Tptpll	1 <sup>a</sup>	8.2	59	4.8	0.70	19	23	16	142	16	2.2	<0.10	42	<1	180	3.70	3.68	0.22
In	SD-9/1184.8-1185.0/UC	Lexan Tube, Protecore	Tptpll	1	7.9	62	5.4	<0.4	24	16	12	196	12	0.84	<0.10	47	7	240	4.04	4.15	-1.38
In	SD-9/1185.0-1185.3/UC1	Lexan Tube, Protecore	Tptpln	1	—	70	8.6	0.27	18.4	42.4	12	145	18.2	2.4	2.50	—	—	—	4.20	4.24	-0.54
In	SD-9/1234.9-1235.1/UC	Lexan Tube, Protecore	Tptpln	1	7.9	67	8.0	0.50	18	17	16	156	11	1.1	<0.12	42	10	216	4.06	3.60	5.98
In	SD-9/1276.5-1276.8/UC	Lexan Tube, Protecore	Tptpln	1	7.9	67	6.4	0.60	23	29	17	136	10	1.9	<0.16	59	21	292	4.28	3.66	7.80
In	SD-9/1276.8-1277.0/UC	Lexan Tube, Protecore	Tptpln	1	7.6	69	6.9	0.60	23	35	17	165	10	2.0	0.29	67	22	278	4.38	4.31	0.80

Table A-2. Screening Status, Chemistry, and Core Storage Conditions for TSw Pore Waters (Continued)

Screening Status	Sample Name	Storage Condition	Lithophysal Unit	Group # (Rep. Water <sup>a</sup> )	pH	Na (mg/L)	K (mg/L)	Mg (mg/L)	Ca (mg/L)	Cl (mg/L)	SO <sub>4</sub> (mg/L)	HCO <sub>3</sub> (mg/L)	NO <sub>3</sub> (mg/L)	F (mg/L)	Br (mg/L)	SiO <sub>2</sub> (mg/L)	Mn (ug/L)	Sr (ug/L)	Sum of Cations <sup>b</sup>	Sum of Anions <sup>c</sup>	Charge Balance %
In	SD-9/1303.4-1303.9/UC	Lexan Tube, Protecore	Ttptln	1	—	95	11.3	2.30	37	65	28	194	19	4.8	<0.43	54	34	411	6.47	6.15	2.47
Out	ECRB-DS2-1613/13.2-13.4/UC	Aluminum Foil, Lexan Tube, Protecore <sup>2</sup>	Ttptpul	—	—	75.6	6.04	1.01	38.2	37.3	22.9	97	34.5	2.84	<0.07	—	—	—	5.43	3.82	17.37
Out	ECRB-DS2-1613/18.6-18.9/UC	Aluminum Foil, Lexan Tube, Protecore <sup>2</sup>	Ttptpul	—	—	64.2	6.14	0.88	29.9	23.8	19.3	97	31.4	2.49	<0.04	—	—	—	4.51	3.30	15.53
Out	ECRB-DS3-1616/7.1-7.5/UC	Aluminum Foil, Lexan Tube, Protecore <sup>2</sup>	Ttptpul	—	—	50.5	6.07	0.51	19.8	14	15.8	91	27.8	1.76	0.1	55	7	119	3.38	2.76	10.23
Out	ECRB-DS3-1616/8.7-8.9/UC	Aluminum Foil, Lexan Tube, Protecore <sup>2</sup>	Ttptpul	—	—	89.1	8.32	0.82	38.4	38.3	23.9	146	37.5	3.89	<0.08	—	—	—	6.07	4.78	11.90
Out	ECRB-DS3-1616/10.4-10.6/UC	Aluminum Foil, Lexan Tube, Protecore <sup>2</sup>	Ttptpul	—	—	45.5	6.21	0.85	20.2	6.42	8.68	119	13.9	1.19	<0.03	35	6.4	88	3.22	2.60	10.64
Out	ECRB-DS3-1616/11.5-12.5/UC	Aluminum Foil, Lexan Tube, Protecore <sup>2</sup>	Ttptpul	—	—	70.8	7.33	0.88	33.0	23.3	16.6	152	19.1	2.83	<0.04	69	7.3	232	4.99	3.95	11.64
Out	ECRB-SYS-CS400/3.8-4.3/UC	Saran Wrap, Lexan Tube, Protecore	Ttptpul	—	7.3	120	12.5	35.1	240	29	94	—	0.25	3.7	<1	48	410	3580	—	—	—
Out	ECRB-SYS-CS400/5.6-6.2/UC	Saran Wrap, Lexan Tube, Protecore	Ttptpul	—	7.0	89	9.7	15.4	85	21	64	415	8.5	1.7	<1	55	43	1480	9.66	8.95	3.81
Out	ECRB-SYS-CS450/5.3-6.0/UC	Saran Wrap, Lexan Tube, Protecore	Ttptpul	—	6.7	68	17.0	22.9	190	66	147	388	4.8	1.1	0.4	54	100	1240	14.79	11.42	12.86
Out	ECRB-SYS-CS500/12.0-16.7/UC	Saran Wrap, Lexan Tube, Protecore	Ttptpul	—	8.0	57	10.3	19.3	120	54	78	286	6.1	4.8	0.4	49	26	1100	10.34	8.19	11.65
Out	ECRB-SYS-CS600/3.6-4.0/UC	Saran Wrap, Lexan Tube, Protecore	Ttptpul	—	7.5	67	10.4	10.6	81	22	50	346	3.3	2.0	<1	44	39	1750	8.13	7.49	4.12
Out	ECRB-SYS-CS700/5.5-5.8/UC	Saran Wrap, Lexan Tube, Protecore	Ttptpul	—	—	91	13.7	33.0	230	64	146	—	2.8	6.2	<0.1	56	330	2970	18.57	5.22	56.14
Out	ECRB-SYS-CS750/6.2-6.5/UC	Saran Wrap, Lexan Tube, Protecore	Ttptpul	—	7.6	70	8.5	12.9	130	73	78	191	<0.2	1.2	<1	40	54	1160	10.84	6.88	22.36
Out	ECRB-SYS-CS800/4.9-5.6/UC	Saran Wrap, Lexan Tube, Protecore	Ttptpul	—	7.4	53	6.6	11.9	92	20	32	357	0.0	1.6	—	53	34	1140	8.07	7.17	5.94

Table A-2. Screening Status, Chemistry, and Core Storage Conditions for TSw Pore Waters (Continued)

Screening Status	Sample Name	Storage Condition	Lithophysal Unit	Group # (Rep. Water <sup>a</sup> )	pH	Na (mg/L)	K (mg/L)	Mg (mg/L)	Ca (mg/L)	Cl (mg/L)	SO <sub>4</sub> (mg/L)	HCO <sub>3</sub> (mg/L)	NO <sub>3</sub> (mg/L)	F (mg/L)	Br (mg/L)	SiO <sub>2</sub> (mg/L)	Mn (ug/L)	Sr (ug/L)	Sum of Cations <sup>b</sup>	Sum of Anions <sup>c</sup>	Charge Balance %
Out	ECRB-SYS-CS850/5.1-5.6/UC	Saran Wrap, Lexan Tube, Protecore	Tptpul	—	8.1	59	5.9	13.1	63	32	30	280	1.6	2.9	<0.2	46	14	1150	6.97	6.29	5.06
Out	ECRB-SYS-CS900/2.8-3.0/UC	Saran Wrap, Lexan Tube, Protecore	Tptpul	—	—	90	8.7	17.7	142	25	63	349	1.2	0.52	0.60	45	469	3250	12.75	7.78	24.20
Out	ECRB-SYS-CS900/3.0-3.2/UC	Saran Wrap, Lexan Tube, Protecore	Tptpul	—	7.4	127	13.0	28.1	229	66	112	—	5.9	0.73	1.2	43	449	5180	—	—	—
Out	ECRB-SYS-CS900/3.5-4.1/UC	Saran Wrap, Lexan Tube, Protecore	Tptpul	—	7.5	140	13.6	25.8	210	53	88	775	1.9	2.0	0.3	65	470	4090	19.13	16.16	8.41
Out	ECRB-SYS-CS900/5.4-5.9/UC	Saran Wrap, Lexan Tube, Protecore	Tptpul	—	7.7	79	6.9	14.0	110	37	56	216	1.3	1.7	<0.2	54	77	1980	10.30	5.86	27.47
Out	ECRB-SYS-CS950/4.8-5.5/UC	Saran Wrap, Lexan Tube, Protecore	Tptpul	—	7.1	84	7.1	22.6	170	30	67	286	11	4.9	<0.2	58	130	2070	14.23	7.36	31.78
Out	ECRB-SYS-CS950/5.2-5.3/UC	Saran Wrap, Lexan Tube, Protecore	Tptpul	—	7.1	66	6.2	13.6	98	19	37	239	0.27	1.9	<0.2	58	62	1240	9.07	5.33	25.98
Out	ECRB-SYS-CS1000/10.9-11.1/UC	Saran Wrap, Lexan Tube, Protecore	Tptpmn	—	—	72	18.7	53.5	275	29	45	700	4.3	0.87	1.4	64	198	2910	21.80	13.34	24.07
Out	ECRB-SYS-CS1000/11.1-11.6/UC	Saran Wrap, Lexan Tube, Protecore	Tptpmn	—	7.3	79	21.3	54.1	280	18	65	714	5.6	0.59	1.1	57	404	2940	22.47	13.68	24.31
Out	ECRB-SYS-CS1000/12.9-14.0/UC	Saran Wrap, Lexan Tube, Protecore	Tptpmn	—	7.8	47	9.9	21.9	120	22	35	405	17	2.0	<0.1	50	47	1110	10.11	8.37	9.45
Out	ECRB-SYS-CS1000/15.6-15.8/UC	Saran Wrap, Lexan Tube, Protecore	Tptpmn	—	—	110	24.8	44.2	240	29	82	741	9.6	1.3	<0.10	61	201	2170	21.08	14.89	17.21
Out	ECRB-SYS-CS1000/5.4-6.1/UC	Saran Wrap, Lexan Tube, Protecore	Tptpmn	—	8.0	64	13.5	21.6	105	48	41	258	5.9	1.0	2.9	50	158	1010	10.17	6.58	21.40
Out	ECRB-SYS-CS1000/7.3-7.7/UC	Saran Wrap, Lexan Tube, Protecore	Tptpmn	—	7.6	39	7.6	18.1	94	21	36	333	2.6	3.4	<1	42	23	1040	8.09	7.02	7.11
Out	ECRB-SYS-CS1100/3.7-3.8/UC	Saran Wrap, Lexan Tube, Protecore	Tptpmn	—	7.1	110	9.0	23.3	170	17	55	525	24	0.65	<0.10	54	238	3160	15.49	10.65	18.51

Table A-2. Screening Status, Chemistry, and Core Storage Conditions for TSw Pore Waters (Continued)

Screening Status	Sample Name	Storage Condition	Lithophysal Unit	Group # (Rep. Water <sup>a</sup> )	pH	Na (mg/L)	K (mg/L)	Mg (mg/L)	Ca (mg/L)	Cl (mg/L)	SO <sub>4</sub> (mg/L)	HCO <sub>3</sub> (mg/L)	NO <sub>3</sub> (mg/L)	F (mg/L)	Br (mg/L)	SiO <sub>2</sub> (mg/L)	Mn (ug/L)	Sr (ug/L)	Sum of Cations <sup>b</sup>	Sum of Anions <sup>c</sup>	Charge Balance %
Out	ECRB-SYS-CS1150/3.2-3.8/UC	Saran Wrap, Lexan Tube, Protecore	Tptpmn	—	—	130	8.8	6.3	96	33	22	323	24	1.9	<0.10	70	33	1130	11.21	7.17	22.00
Out	ECRB-SYS-CS1250/3.4-4.0/UC	Saran Wrap, Lexan Tube, Protecore	Tptpmn	—	7.5	83	13.7	23.5	160	25	60	464	1.3	2.1	—	54	200	1390	13.91	9.69	17.88
Out	ECRB-SYS-CS1250/5.0-5.7/UC	Saran Wrap, Lexan Tube, Protecore	Tptpmn	—	7.7	79	11.2	7.9	55	50	21	—	25	3.0	0.2	59	18	480	—	—	—
Out	ECRB-SYS-CS1500/10.0-12.1/UC	Saran Wrap, Lexan Tube, Protecore	Tptpll	—	8.1	120	11.1	16.4	130	97	97	349	0.52	1.4	0.91	45.7	220	1250	13.37	10.56	11.75
Out	ECRB-SYS-CS2000/16.3-16.5/UC	Saran Wrap, Lexan Tube, Protecore	Tptpll	—	7.4	120	6.1	3.3	81	24	31	362	0.41	6.0	<0.2	42	130	1260	9.72	7.58	12.38
Out	ECRB-SYS-CS2000/16.5-21.1/UC	Saran Wrap, Lexan Tube, Protecore	Tptpll	—	7.4	130	10.6	5.3	82	26	39	382	4.2	11	<0.2	48	58	1390	10.49	8.45	10.74
Out	ECRB-SYS-CS2000/3.3-3.8/UC	Saran Wrap, Lexan Tube, Protecore	Tptpll	—	—	204	20.3	7.1	170	38	76	639	0	3.9	0.96	64	120	3702	18.54	13.33	16.35
Out	ECRB-SYS-CS2000/3.95-4.1/UC	Saran Wrap, Lexan Tube, Protecore	Tptpll	—	7.8	116	11.1	2.8	88	20	35	329	2.0	7.7	0.22	39	89	1460	9.98	7.12	16.73
Out	ECRB-SYS-CS2150/5.5-6.1/UC	Saran Wrap, Lexan Tube, Protecore	Tptpll	—	7.6	83	6.9	8.3	98	27	48	265	1.2	5.3	<0.2	52	38	1110	9.39	6.40	18.90
Out	ECRB-SYS-CS2250/5.2-5.6/UC	Saran Wrap, Lexan Tube, Protecore	Tptpll	—	8.0	74	9.1	10.1	87	24	27	384	1.3	1.1	<0.10	54	69	690	8.64	7.61	6.33
Out	ECRB-SYS-CS2300/4.3-4.9/UC	Saran Wrap, Lexan Tube, Protecore	Tptpll	—	7.9	98	12.5	10.2	73	23	34	340	0.9	1.7	<0.1	43	260	590	9.08	7.03	12.69
Out	ECRB-SYS-CS2300/6.1-6.7/UC	Saran Wrap, Lexan Tube, Protecore	Tptpll	—	8.2	96	12.7	9.3	65	20	13	434	1.4	1.0	<0.10	49	49	610	8.52	8.02	3.03
Out	ECRB-SYS-CS2350/5.0-5.7/UC	Saran Wrap, Lexan Tube, Protecore	Tptpll	—	—	110	11.2	10.8	58	45	22	—	6.3	5.9	<0.10	46.1	54	750	—	—	—
Out	ESF-SAD-GTB#1/119.4-120.0/UC	Saran Wrap, Lexan Tube, Protecore	Tptpmn	—	—	69	19.2	12.0	73	69	46	266	3.9	1.5	0.40	51	95	660	8.14	7.41	4.71

Table A-2. Screening Status, Chemistry, and Core Storage Conditions for TSw Pore Waters (Continued)

Screening Status	Sample Name	Storage Condition	Lithophysal Unit	Group # (Rep. Water <sup>a</sup> )	pH	Na (mg/L)	K (mg/L)	Mg (mg/L)	Ca (mg/L)	Cl (mg/L)	SO <sub>4</sub> (mg/L)	HCO <sub>3</sub> (mg/L)	NO <sub>3</sub> (mg/L)	F (mg/L)	Br (mg/L)	SiO <sub>2</sub> (mg/L)	Mn (ug/L)	Sr (ug/L)	Sum of Cations <sup>b</sup>	Sum of Anions <sup>c</sup>	Charge Balance %
Out	ESF-SAD-GTB#1/126.1-126.4/UC	Saran Wrap, Lexan Tube, Protecore	Tptpmn	—	—	100	22.4	23.3	170	133	66	427	6.2	1.2	0.63	54	310	1680	15.36	12.29	11.12
Out	ESF-SAD-GTB#1/194.2-195.2/UC	Saran Wrap, Lexan Tube, Protecore	Tptpmn	—	8.0	97	24.7	35.5	230	110	115	545	1.5	1.5	0.89	66	820	2350	19.30	14.53	14.10
Out	ESF-SAD-GTB#1/195.4-196.7/UC	Saran Wrap, Lexan Tube, Protecore	Tptpmn	—	7.6	81	21.2	29.0	190	97	79	501	3.7	1.4	0.57	62	390	1930	15.98	12.72	11.33
Out	ESF-SAD-GTB#1/199.0-199.3/UC	Saran Wrap, Lexan Tube, Protecore	Tptpmn	—	—	161	30.6	38.2	268	180	112	706	35.1	1.4	—	—	—	—	24.30	19.62	10.66
Out	HD-PERM-2/19.3-19.7/UC	Lexan Tube, Protecore	Tptpmn	—	—	101	15.7	17.2	113	133	129	259	28.8	1.8	—	—	—	—	11.85	11.24	2.63
Out	HD-PERM-2/34.5-34.9/UC	Lexan Tube, Protecore	Tptpmn	—	—	110	17.1	17.8	143	128	128	368	18.5	1.5	—	—	—	—	13.82	12.68	4.30
Out	HD-PERM-2/61.7-62.3/UC	Lexan Tube, Protecore	Tptpmn	—	—	86.7	16.9	8.2	89	86.5	76.2	236	37.3	1.7	—	—	—	—	9.32	8.59	4.10
Out	SD-9/670.5-670.6/UC	Saran Wrap, Lexan Tube, Protecore	Tptpul	—	—	72	8.4	9.0	81	46	56	—	28	2.8	0.30	53	42	500	—	—	—
Out	SD-9/990.4-991.7/UC	Lexan Tube, Protecore	Tptpll	—	7.9	84	7.9	0.90	56	23	10	313	17	2.5	<0.2	50	21	420	6.73	6.39	2.60
Out	SD-9/1184.0-1184.2/UC	Lexan Tube, Protecore	Tptpll	—	7.7	92	7.6	1.9	44	44	17	221	17	1.7	<0.10	45	32	450	6.56	5.58	8.06
Out	SD-9/1236.4-1236.8/UC	Lexan Tube, Protecore	Tptpln	—	7.5	100	8.4	4.9	51	77	21	210	12	3.6	<0.10	54	20	620	7.53	6.43	7.83
Out	SD-9/1275.6-1276.0/UC	Lexan Tube, Protecore	Tptpln	—	7.5	81	7.7	2.5	42	61	20	146	8.5	3.7	<0.10	38	17	510	6.03	4.86	10.76
Out	SD-9/1330.4-1330.7/UC	Lexan Tube, Protecore	Tptpln	—	7.2	130	9.5	7.5	73	133	35	245	15	5.0	0.54	55	31	960	10.18	9.00	6.15
Out	SD-12/1053.7-1054.1 UC-1	Saran Wrap, Lexan Tube, Protecore	Tptpll	—	7.7	122	11.9	23.9	75	180	32	308	4.2	3.8	<0.10	43	58	849	11.34	11.06	1.25
Excluded <sup>1</sup>	ESF-HD-ChemSamp-1/26.1-26.9/UC	ND	Tptpmn	—	7.6	53	8.4	18.0	82	71	88	254	22	0.91	0.24	49	29	893	8.11	8.40	-1.73
Excluded <sup>1</sup>	ESF-HD-ChemSamp-1/28.8-29.7/UC	ND	Tptpmn	—	—	69	10.7	16.5	84	45	70	162	20	0.83	<0.20	49	46	833	8.84	5.75	21.22
Excluded <sup>1</sup>	ESF-HD-ChemSamp-1/34.6-35.4/UC	ND	Tptpmn	—	—	63	10.9	12.7	56	48	59	63	38	1.8	<0.10	47	49	566	6.87	4.32	22.77
Excluded <sup>1</sup>	ESF-HD-ChemSamp-1/37.1-37.2/UC	ND	Tptpmn	—	—	66	13.6	11.6	57	79	62	192	29	1.7	<0.30	56	52	553	7.03	7.22	-1.35
Excluded <sup>1</sup>	ESF-HD-ChemSamp-3/104.6-105.3/UC	ND	Tptpmn	—	7.9	39	5.2	2.0	13	27	23	45	6.0	0.84	<0.10	28	16	148	2.65	2.12	11.06
Excluded <sup>1</sup>	ESF-HD-ChemSamp-3/108.4-109.0/UC	ND	Tptpmn	—	—	61	7.9	4.2	26	58	44	104	11	0.80	<0.10	36	11	405	4.51	4.48	0.35
Excluded <sup>1</sup>	ESF-HD-ChemSamp-3/111.8-112.0/UC	ND	Tptpmn	—	—	108	18.3	9.6	49	66	75	—	18	1.3	<0.40	65	21	649	—	—	—
Excluded <sup>1</sup>	ESF-HD-ChemSamp-3/113.1-113.8/UC	ND	Tptpmn	—	—	103	15.2	11.5	63	83	115	212	25	1.2	0.61	73	26	826	8.98	8.68	1.71

Table A-2. Screening Status, Chemistry, and Core Storage Conditions for TSw Pore Waters (Continued)

Screening Status	Sample Name	Storage Condition	Lithophysal Unit	Group # (Rep. Water <sup>a</sup> )	pH	Na (mg/L)	K (mg/L)	Mg (mg/L)	Ca (mg/L)	Cl (mg/L)	SO <sub>4</sub> (mg/L)	HCO <sub>3</sub> (mg/L)	NO <sub>3</sub> (mg/L)	F (mg/L)	Br (mg/L)	SiO <sub>2</sub> (mg/L)	Mn (ug/L)	Sr (ug/L)	Sum of Cations <sup>b</sup>	Sum of Anions <sup>c</sup>	Charge Balance %
Excluded <sup>1</sup>	ESF-HD-ChemSamp-3/115.0-115.6/UC	ND	Tptpmn	—	—	89	15.7	9.2	46	66	58	228	17	1.0	<0.53	64	65	532	7.34	7.13	1.42
Excluded <sup>1</sup>	ESF-HD-ChemSamp-3/127.1-128.0/UC	ND	Tptpmn	—	—	85	13.1	10.8	55	63	79	235	18	1.4	0.67	59	32	649	7.68	7.64	0.28
Excluded <sup>1</sup>	ESF-HD-ChemSamp-3/33.9-34.4/UC	ND	Tptpmn	—	—	45	6.4	6.1	29	41	51	88	18	1.2	0.36	45	18	323	4.08	4.01	0.79
Excluded <sup>1</sup>	ESF-HD-ChemSamp-3/34.4-34.5/UC	ND	Tptpmn	—	7.6	40	5.3	5.4	28	41	51	72	18	1.2	0.19	43	16	312	3.72	3.75	-0.37
Excluded <sup>1</sup>	ESF-HD-ChemSamp-3/36.5-37.5/UC	ND	Tptpmn	—	7.9	96	14.0	8.6	62	107	128	143	39	1.7	0.37	51	42	714	8.35	8.75	-2.30
Excluded <sup>1</sup>	ESF-HD-ChemSamp-3/38.2-39.1/UC	ND	Tptpmn	—	—	116	19.7	11.0	51	34	17	145	5.9	0.45	<0.10	46	66	552	9.01	3.81	40.59
Excluded <sup>1</sup>	ESF-HD-ChemSamp-3/42.3-42.8/UC	ND	Tptpmn	—	8.0	66	8.8	1.5	21	30	30	146	10	0.79	0.13	57	—	237	4.27	4.07	2.47
Excluded <sup>1</sup>	ESF-HD-ChemSamp-3/46.0-46.3/UC	ND	Tptpmn	—	7.8	30	4.9	1.2	6.9	12	8.8	—	5.3	1.3	<0.17	33	15	70	—	—	—
Excluded <sup>1</sup>	ESF-HD-ChemSamp-3/46.3-46.9/UC	ND	Tptpmn	—	7.9	51	6.9	3.4	17	27	19	118	7.9	1.0	0.15	53	6.2	171	3.53	3.27	3.76
Excluded <sup>2</sup>	SD-6/1509.9 – 1510.3/UC1	ND	Tptpv2	—	7.7	98.9	8.3	2.6	65.8	98.7	28	178	1.8	14.7	—	54.5	—	—	8.01	7.09	6.13
Excluded <sup>3</sup>	SD-9 /669.8-669.9/UC1	ND	Tptpul	—	8.5	44	5.8	6.5	50.2	43.8	42.2	205	20.5	7.2	0.00	46	—	—	5.11	6.18	-9.50
Excluded <sup>3</sup>	SD-9/ 669.7-669.8/UC1	ND	Tptpul	—	8.5	68	11.9	7.5	61.8	61.8	44.6	185	21.0	10.4	0.00	49	—	—	6.96	6.59	2.73
Excluded <sup>4</sup>	SD-9/1095.6-1096.0/UC	ND	Tptpll	—	7.6	110	8.1	7.10	72	—	—	—	—	—	—	52	35	630	—	—	—
Excluded <sup>3</sup>	SD-9/669.0-669.1/UC1	ND	Tptpul	—	8.3	59	10.0	5.6	43.8	53.3	47.1	143	29.5	7.5	0.10	53	—	—	5.47	5.70	-2.06
Excluded <sup>4</sup>	UZ14-1258.5-1258.8/UP-1	ND	Tptpln	—	—	67	—	3.7	43	88	19	170	16	—	—	—	—	—	—	—	—
Excluded <sup>4</sup>	UZ14-1277.4-1277.7/UP-1	ND	Tptpln	—	—	49	—	4.5	62	87	45	170	17	—	—	—	—	—	—	—	—
Excluded <sup>4</sup>	UZ14-1277.7-1278.0/UP-1	ND	Tptpln	—	—	45	—	5.1	74	130	38	170	15	—	—	—	—	—	—	—	—
Excluded <sup>5</sup>	UZ14A/384.6	ND	Tptpln	—	7.6	39	5.6	1.8	23	7.9	14.3	150	8.6	—	—	34.2	—	—	3.14	3.12	0.29
Excluded <sup>5</sup>	UZ14A2/384.6	ND	Tptpln	—	7.8	38	3.9	1.8	24	9.1	13.8	148.8	12.5	—	—	36.4	—	—	3.10	3.18	-1.37
Excluded <sup>5</sup>	UZ14B/387.68	ND	Tptpln	—	8.1	40	4.4	2.7	31	8.3	16.3	147.6	16.9	—	—	51.4	—	—	3.62	3.27	5.18
Excluded <sup>5</sup>	UZ14C/390.75	ND	Tptpv	—	8.3	88	5.8	4.1	45	15.5	223	106.1	0	—	—	7.7	—	—	6.56	6.82	-1.94
Excluded <sup>5</sup>	UZ14D/390.75	ND	Tptpv	—	—	35	4.1	2.5	31	7	24.2	146.4	17.1	—	—	40.7	—	—	3.38	3.38	0.05
Excluded <sup>5</sup>	UZ14PT-1/390.75	ND	Tptpv	—	—	40	6.3	3.1	37	7.2	57.3	144	12.7	—	—	21.4	—	—	4.00	3.96	0.52
Excluded <sup>5</sup>	UZ14PT-2/390.75	ND	Tptpv	—	—	35	3.3	2.4	30	7	22.9	144	15.4	—	—	25.7	—	—	3.30	3.28	0.29
Excluded <sup>5</sup>	UZ14PT-4/390.75	ND	Tptpv	—	—	34	1.8	2.1	27	6.7	14.1	141.5	14.5	—	—	32.1	—	—	3.05	3.04	0.16
Excluded <sup>4</sup>	UZ16-1166.19-1166.47/UP-1	ND	Tptpv2	—	8.1	83.6	—	13.7	28.9	82	28	196	17	—	—	—	—	—	—	—	—
Excluded <sup>4</sup>	UZ16-952.6-952.9/UP-1	ND	Tptpln	—	8.2	99.5	—	13.7	2.2	81	34	179	30	—	—	—	—	—	—	—	—

**Screening Status (Column 1) Footnotes:**

- <sup>1</sup> Thermally perturbed; heated block of Drift-Scale Test.
- <sup>2</sup> Base of TSw, below repository horizon.
- <sup>3</sup> Samples collected prior to establishment of QA procedures.
- <sup>4</sup> Analysis incomplete (missing other than pH, HCO<sub>3</sub><sup>-</sup>, or SiO<sub>2</sub>).
- <sup>5</sup> Perched water in Tptpv and base of Tptpln (below repository level). Note that depths (these samples only) are given in meters, not feet.

**Storage Condition (Column 3) Footnotes:**

- <sup>1</sup> Cleaned split sleeves, shoe, and inner barrel with Liquinox and DI water. Cores handled with sterile gloves.
- <sup>2</sup> Core bits, barrels and sleeves cleaned with Liquinox and DI water. Cores handled with sterile gloves.
- ND = Not Determined.

**General Footnotes:**

- <sup>a</sup> Representative water used in NFC model to represent the four water groups (1, 2, 3, and 4).
- <sup>b</sup> Cation equivalents calculated using Ca<sup>2+</sup>, Mg<sup>2+</sup>, Na<sup>+</sup>, K<sup>+</sup>, and Sr<sup>2+</sup>. Mn not used due to very low concentrations.
- <sup>c</sup> Anion equivalents calculated using = Cl<sup>-</sup>, SO<sub>4</sub><sup>2-</sup>, HCO<sub>3</sub><sup>-</sup>, NO<sub>3</sub><sup>-</sup>, and F<sup>-</sup>. Br not used due to very low concentrations.
- <sup>d</sup> Anion and cation equivalents and charge balance are not calculated if a major charged anion or cation (e.g., HCO<sub>3</sub><sup>-</sup> or K<sup>+</sup>) was not analyzed.

ENCLOSURE 1

Response Tracking Number: 00215-00-000

RAI: 3.2.2.1.3.3-001

**APPENDIX B**

**CONTENTS OF *WATER\_SAMPLE\_LOCATIONS\_EV.DAT***

ENCLOSURE 1

Response Tracking Number: 00215-00-000

RAI: 3.2.2.1.3.3-001

```

# Type: scattered data
# Version: 7
# Description: from RAI porewater spreadsheet_tjv.xls (convert OK)
# Format: free
# Field: 1 x
# Field: 2 y
# Field: 3 z feet
# Field: 4 wellid non-numeric
# Projection: State Plane
# Zone: 2702 -- Nevada (Central)
# Units: feet
# Ellipsoid: Clarke 1866
# End:
##Feet - (X) Feet - (Y) Feet; Ground Elevation MSL-(Z) Sample Name
559920.764 765346.808 3629.423 "ECRB-DS3-1616/7.5-7.7/UC"
559920.764 765346.808 3629.423 "ECRB-DS3-1616/7.7-7.9/UC"
559920.764 765346.808 3629.423 "ECRB-DS3-1616/7.9-8.0/UC"
559920.764 765346.808 3629.423 "ECRB-DS3-1616/8.0-8.1/UC"
559920.764 765346.808 3629.423 "ECRB-DS3-1616/9.6-9.8/UC"
559920.764 765346.808 3629.423 "ECRB-DS3-1616/9.8-10.1/UC"
559920.764 765346.808 3629.423 "ECRB-DS3-1616/10.1-10.4/UC"
559920.764 765346.808 3629.423 "ECRB-DS3-1616/10.6-11.0/UC"
559920.764 765346.808 3629.423 "ECRB-DS3-1616/12.5-12.7/UC"
559920.764 765346.808 3629.423 "ECRB-DS3-1616/12.7-13.3/UC"
562501.618 767933.563 3461.742 "ESF-HD-PERM-1"
562500.618 767930.783 3464.239 "ESF-HD-PERM-2"
562498.820 767924.941 3461.788 "ESF-HD-PERM-3"
562184.839 756735.554 3687.454 "ESF-THERMALK-017/16.6-17.2/UC"
562184.839 756735.554 3687.454 "ESF-THERMALK-017/22.3-22.9/UC"
562184.839 756735.554 3687.454 "ESF-THERMALK-017/22.9-23.0/UC"
562184.839 756735.554 3687.454 "ESF-THERMALK-017/26.3-26.5/UC"
562184.839 756735.554 3687.454 "ESF-THERMALK-017/26.5-26.9/UC"
562186.680 756735.591 3686.801 "ESF-THERMALK-019/19.2-19.5/UC"
562186.680 756735.591 3686.801 "ESF-THERMALK-019/19.5-19.7/UC"
562498.820 767924.941 3461.788 "HD-PERM-3/22.4-23.0/UC"
562498.820 767924.941 3461.788 "HD-PERM-3/56.7-57.1/UC"
562983.990 768880.110 3367.87 "NRG-7/7A/839.3-839.8/UC"
561818.02 767998.49 3603.54 "SD-9/669.1-669.2/UC"
561818.02 767998.49 3280.94 "SD-9/991.7-992.1/UC"
561818.02 767998.49 3212.54 "SD-9/1060.1-1060.5/UC"
561818.02 767998.49 3152.94 "SD-9/1119.7-1119.9/UC"
561818.02 767998.49 3087.94 "SD-9/1184.7-1184.8/UC"
561818.02 767998.49 3087.84 "SD-9/1184.8-1185.0/UC"
561818.02 767998.49 3087.64 "SD-9/1185.0-1185.3/UC1"
561818.02 767998.49 3037.74 "SD-9/1234.9-1235.1/UC"
561818.02 767998.49 2996.14 "SD-9/1276.5-1276.8/UC"
561818.02 767998.49 2995.84 "SD-9/1276.8-1277.0/UC"
561818.02 767998.49 2969.24 "SD-9/1303.4-1303.9/UC"
559927.769 765352.982 3635.948 "ECRB-DS2-1613/13.2-13.4/UC"
559927.769 765352.982 3635.948 "ECRB-DS2-1613/18.6-18.9/UC"
559920.764 765346.808 3629.423 "ECRB-DS3-1616/7.1-7.5/UC"
559920.764 765346.808 3629.423 "ECRB-DS3-1616/8.7-8.9/UC"
559920.764 765346.808 3629.423 "ECRB-DS3-1616/10.4-10.6/UC"
559920.764 765346.808 3629.423 "ECRB-DS3-1616/11.5-12.5/UC"
562935.571 767956.024 3573.494 "ECRB-SYS-CS400/3.8-4.3/UC"

```

562935.571	767956.024	3573.494	"ECRB-SYS-CS400/5.6-6.2/UC"
562812.730	767849.337	3576.457	"ECRB-SYS-CS450/5.3-6.0/UC"
562689.304	767742.126	3579.724	"ECRB-SYS-CS500/12.0-16.7/UC"
562439.692	767525.269	3585.925	"ECRB-SYS-CS600/3.6-4.0/UC"
562191.709	767309.800	3591.706	"ECRB-SYS-CS700/5.5-5.8/UC"
562071.486	767204.997	3594.646	"ECRB-SYS-CS750/6.2-6.5/UC"
561946.522	767096.457	3597.441	"ECRB-SYS-CS800/4.9-5.6/UC"
561823.009	766989.180	3599.800	"ECRB-SYS-CS850 5.1-5.6/UC"
561696.804	766879.478	3602.520	"ECRB-SYS-CS900/2.8-3.0/UC"
561696.804	766879.478	3602.520	"ECRB-SYS-CS900/3.0-3.2/UC"
561696.804	766879.478	3602.520	"ECRB-SYS-CS900/3.5-4.1/UC"
561696.804	766879.478	3602.520	"ECRB-SYS-CS900/5.4-5.9/UC"
561574.856	766773.524	3604.554	"ECRB-SYS-CS950/4.8-5.5/UC"
561574.856	766773.524	3604.554	"ECRB-SYS-CS950/5.2-5.3/UC"
561450.650	766665.686	3607.159	"ECRB-SYS-CS1000/10.9-11.1/UC"
561450.650	766665.686	3607.159	"ECRB-SYS-CS1000/11.1-11.6/UC"
561450.650	766665.686	3607.159	"ECRB-SYS-CS1000/12.9-14.0/UC"
561450.650	766665.686	3607.159	"ECRB-SYS-CS1000/15.6-15.8/UC"
561450.650	766665.686	3607.159	"ECRB-SYS-CS1000/5.4-6.1/UC"
561450.650	766665.686	3607.159	"ECRB-SYS-CS1000/7.3-7.7/UC"
561202.671	766449.852	3612.136	"ECRB-SYS-CS1100/3.7-3.8/UC"
561079.432	766342.661	3614.311	"ECRB-SYS-CS1150/3.2-3.8/UC"
560831.506	766127.159	3619.459	"ECRB-SYS-CS1250/3.4-4.0/UC"
560831.506	766127.159	3619.459	"ECRB-SYS-CS1250/5.0-5.7/UC"
560215.988	765592.185	3631.414	"ECRB-SYS-CS1500/10.0-12.1/UC"
558977.608	764515.499	3647.677	"ECRB-SYS-CS2000/16.3-16.5/UC"
558977.608	764515.499	3647.677	"ECRB-SYS-CS2000/16.5-21.1/UC"
558977.608	764515.499	3647.677	"ECRB-SYS-CS2000/3.3-3.8/UC"
558977.608	764515.499	3647.677	"ECRB-SYS-CS2000/3.95-4.1/UC"
558606.703	764193.005	3652.388	"ECRB-SYS-CS2150/5.5-6.1/UC"
558356.299	763975.394	3655.512	"ECRB-SYS-CS2250/5.2-5.6/UC"
558232.283	763867.782	3656.824	"ECRB-SYS-CS2300/4.3-4.9/UC"
558232.283	763867.782	3656.824	"ECRB-SYS-CS2300/6.1-6.7/UC"
558104.987	763763.451	3658.465	"ECRB-SYS-CS2350/5.0-5.7/UC"
562159.941	760597.080	3623.819	"ESF-SAD-GTB#1/119.4-120.0/UC"
562159.941	760597.080	3623.819	"ESF-SAD-GTB#1/126.1-126.4/UC"
562159.941	760597.080	3623.819	"ESF-SAD-GTB#1/194.2-195.2/UC"
562159.941	760597.080	3623.819	"ESF-SAD-GTB#1/195.4-196.7/UC"
562159.941	760597.080	3623.819	"ESF-SAD-GTB#1/199.0-199.3/UC"
562500.618	767930.783	3464.239	"HD-PERM-2/19.3-19.7/UC"
562500.618	767930.783	3464.239	"HD-PERM-2/34.5-34.9/UC"
562500.618	767930.783	3464.239	"HD-PERM-2/61.7-62.3/UC"
561818.02	767998.49	3602.14	"SD-9/670.5-670.6/UC"
561818.02	767998.49	3282.24	"SD-9/990.4-991.7/UC"
561818.02	767998.49	3088.64	"SD-9/1184.0-1184.2/UC"
561818.02	767998.49	3036.24	"SD-9/1236.4-1236.8/UC"
561818.02	767998.49	2997.04	"SD-9/1275.6-1276.0/UC"
561818.02	767998.49	2942.24	"SD-9/1330.4-1330.7/UC"
561605.608	761956.559	3289.12	"SD-12/1053.7-1054.1 UC-1"
562365.545	767846.342	3472.001	"ESF-HD-ChemSamp-1/26.1-26.9/UC"
562365.545	767846.342	3472.001	"ESF-HD-ChemSamp-1/28.8-29.7/UC"
562365.545	767846.342	3472.001	"ESF-HD-ChemSamp-1/34.6-35.4/UC"
562365.545	767846.342	3472.001	"ESF-HD-ChemSamp-1/37.1-37.2/UC"
562363.346	767842.723	3462.762	"ESF-HD-ChemSamp-3/104.6-105.3/UC"
562363.346	767842.723	3462.762	"ESF-HD-ChemSamp-3/108.4-109.0/UC"

ENCLOSURE 1

Response Tracking Number: 00215-00-000

RAI: 3.2.2.1.3.3-001

562363.346	767842.723	3462.762	"ESF-HD-ChemSamp-3/111.8-112.0/UC"
562363.346	767842.723	3462.762	"ESF-HD-ChemSamp-3/113.1-113.8/UC"
562363.346	767842.723	3462.762	"ESF-HD-ChemSamp-3/115.0-115.6/UC"
562363.346	767842.723	3462.762	"ESF-HD-ChemSamp-3/127.1-128.0/UC"
562363.346	767842.723	3462.762	"ESF-HD-ChemSamp-3/33.9-34.4/UC"
562363.346	767842.723	3462.762	"ESF-HD-ChemSamp-3/34.4-34.5/UC"
562363.346	767842.723	3462.762	"ESF-HD-ChemSamp-3/36.5-37.5/UC"
562363.346	767842.723	3462.762	"ESF-HD-ChemSamp-3/38.2-39.1/UC"
562363.346	767842.723	3462.762	"ESF-HD-ChemSamp-3/42.3-42.8/UC"
562363.346	767842.723	3462.762	"ESF-HD-ChemSamp-3/46.0-46.3/UC"
562363.346	767842.723	3462.762	"ESF-HD-ChemSamp-3/46.3-46.9/UC"
558,607.68	762,421.39	3395.42	"SD-6/1509.9 - 1510.3/UC1"
561818.02	767998.49	3602.84	"SD-9 /669.8-669.9/UC1"
561818.02	767998.49	3602.94	"SD-9/ 669.7-669.8/UC1"
561818.02	767998.49	3177.04	"SD-9/1095.6-1096.0/UC"
561818.02	767998.49	3603.64	"SD-9/669.0-669.1/UC1"
560141.57	771309.80	3166.90	"UZ14-1258.5-1258.8/UP-1"
560141.57	771309.80	3148.00	"UZ14-1277.4-1277.7/UP-1"
560141.57	771309.80	3147.70	"UZ14-1277.7-1278.0/UP-1"
560141.57	771309.80	4040.80	"UZ14A/384.6"
560141.57	771309.80	4040.80	"UZ14A2/384.6"
560141.57	771309.80	4037.72	"UZ14B/387.68"
560141.57	771309.80	4034.65	"UZ14C/390.75"
560141.57	771309.80	4034.65	"UZ14D/390.75"
560141.57	771309.80	4034.65	"UZ14PT-1/390.75"
560141.57	771309.80	4034.65	"UZ14PT-2/390.75"
560141.57	771309.80	4034.65	"UZ14PT-4/390.75"
564857.490	760535.130	2834.29	"UZ16-1166.19-1166.47/UP-1"
564857.490	760535.130	3047.88	"UZ16-952.6-952.9/UP-1"

**RAI: Volume 3, Chapter 2.2.1.3.3, First Set, Number 2:**

Provide the following additional technical bases to demonstrate that the near-field chemistry (NFC) model adequately calculates a range of water compositions in the natural system:

Compare the results of the DOE NFC model with the results of the DOE thermal-hydrological-chemical (THC) seepage model. This comparison should include, as a minimum, the following parameters as a function of time:

- Calcium
- pH
- Ionic strength
- Chloride
- Nitrate
- Chloride:nitrate ratio
- Partial pressure of carbon dioxide
- Any additional component that DOE concludes is significant to the evaluation of near-field chemistry in the performance assessment.

In addition, identify and quantify the effect of the alternative conceptual model on localized corrosion and the calculation of repository performance.

**Basis:** DOE uses the NFC model for TSPA to calculate the interaction between percolating pore waters and the rock matrix to represent the chemistries of fluids entering drifts (SAR Section 2.3.5.3.3.5.3). Prior to using the NFC model, the THC seepage model was used to predict the chemistry of seepage water entering the drifts (SAR Section 2.3.5.3.3.5.3). SAR Section 2.3.5.3.3.4 presents the limitations of the NFC model such as "... the model domain is implemented as plug flow, rather than modeling discrete fracture and matrix interactions." SAR Section 2.3.5.3.3.5.3 describes numerous significant differences in terms of implementation between the NFC model and its predecessor, the THC seepage model. This section also compares the two models using the feldspar dissolution rate and activation energy ( $E_a$ ) for feldspar dissolution from the THC seepage model. The feldspar dissolution rate from the THC seepage model is about seven times higher than the NFC model at 23.4°C and about 21 times the NFC model rate at 96°C, as a result of the higher activation energy in the THC seepage model. Using the same values for the feldspar dissolution rate and the  $E_a$  for feldspar dissolution is appropriate for comparing the two model codes. However, the differences in the outputs of the two codes resulting from using their unique and individual feldspar dissolution rates and  $E_a$  for feldspar dissolution cannot be determined from the results presented in this section (SAR Figures 2.3.5-23 and 2.3.5-24).

As presented, the NFC model and the THC seepage model appear to present alternative conceptual approaches to calculating seepage water chemistry. Although SEIS Table 5-1 acknowledges and attributes a small decrease in dose to refinements in the predicted ground water chemistry when the newer NFC model was implemented, this decrease is not discussed in SAR Section 2.3.5.3.3.4. The requested information is needed for NRC review of the technical bases presented in the SAR to support the use of the NFC model for TSPA and for the review of the potential effects of the NFC model on performance.

## 1. RESPONSE

### 1.1 INTRODUCTION

A comparison of values between the near-field chemistry (NFC) model and the thermal-hydrologic-chemical (THC) seepage model was carried out as part of the validation of the NFC model (SAR Section 2.3.5.3.3.5.3), with a NFC model simulation that used an ambient feldspar dissolution rate ( $R_{feld}$ ) and activation energy ( $E_a$ ) adjusted to match those used in the THC seepage model. The RAI requests that the two models be compared, this time with NFC simulations using the same  $R_{feld}$  and  $E_a$  as the total system performance assessment (TSPA) baseline calculations. In such a comparison, seepage water compositions predicted by the two models would clearly differ due to the differences in the feldspar dissolution rate parameters. Based on the clarification call on March 17, 2009, and on the following response, the quantitative comparison of the THC seepage model and NFC model outputs originally requested by this RAI is not directly germane to demonstrating that the NFC model adequately calculates a range of water compositions in the natural system, and alternative information is provided. Confidence that the NFC model generates an appropriate range of water compositions is provided by showing that the feldspar dissolution rate parameters used by the NFC model are appropriate for use at Yucca Mountain, and that other model uncertainties are adequately captured and propagated into the total system performance assessment (TSPA) model.

Additional information pertaining to the NFC model and its implementation is provided for the purpose of demonstrating the requested additional confidence in the model. In particular, the implementation of the NFC model, its inputs and outputs, and how uncertainties in initial water chemistry are propagated through the model to the seepage evaporation abstraction and to the TSPA model are described. The response also provides details associated with the pretreatment of the four representative water compositions used in the NFC model (e.g., charge balancing, and equilibration at a  $p\text{CO}_2$  of  $10^{-3}$  bars) and the resulting changes in composition. Much of the uncertainty in water compositions is not incorporated in the NFC model because the TSPA never calculates seepage water compositions, but is propagated later through the seepage evaporation abstraction, which predicts in-drift water compositions. To demonstrate that an adequate range of water compositions is predicted under ambient and near-ambient conditions, results from TSPA model baseline simulations are summarized below. These results are the predicted in-drift water chemistries at 1,000,000 years after closure, after the drift temperatures have largely returned to ambient, and they are compared to the site characterization data for pore-water compositions.

The RAI requests that DOE identify and quantify the effect of using “the alternative conceptual model [the THC seepage model] on localized corrosion and the calculation of repository performance.” This response details the reasons why the THC seepage model has been replaced by the NFC model in the TSPA—largely because the THC seepage model does not capture the full ranges of uncertainty and spatial variability in parameters that affect seepage composition. The THC seepage model is used primarily to support appropriate screening of features, events, and processes (FEPs), for evaluating the effects of near-field THC effects and dryout around the drift on water chemistry and on rock hydrologic properties, during the early thermal period (a few thousand years). It evaluates those effects for a few representative cases comprising a more limited sample of parametric uncertainty and variability than what is used with the NFC model in the TSPA model.

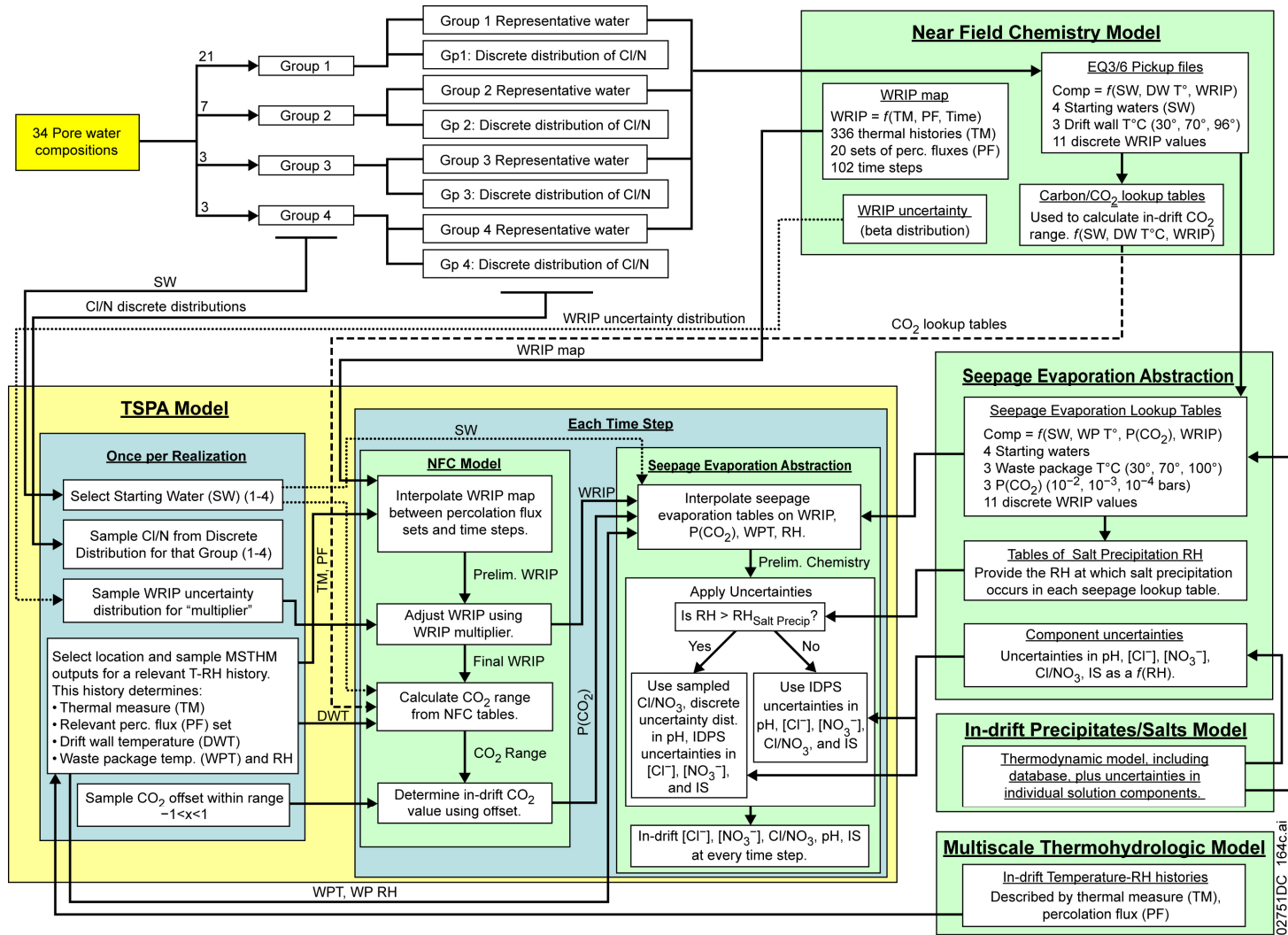
Also, because the basis for this RAI specifically discusses the differences in the feldspar dissolution rates used in the two models, this response evaluates the point estimates for  $R_{feld}$  and  $E_a$  used in the THC seepage model and compares them to the more representative range used with the NFC model.

Finally, this response addresses a statement in the RAI basis concerning differences in doses predicted with the THC seepage model used in the TSPA for the Final Environmental Impact Statement (FEIS) and the NFC model used in the TSPA for the Supplemental Environmental Impact Statement (SEIS). In the SEIS, a slight reduction in dose releases is attributed to the change from the THC seepage model to the NFC model in the TSPA calculations. The version of the THC seepage model that was used in FEIS is different than the current version, and the statement in the SEIS does not apply to the current THC seepage model.

## **1.2 INTEGRATION OF THE NEAR-FIELD CHEMISTRY MODEL WITH THE SEEPAGE EVAPORATION ABSTRACTION AND WITH THE TSPA MODEL**

The integration of the NFC model with the seepage evaporation abstraction and within TSPA is illustrated in Figure 1. Inputs to the NFC model (other than parameter values) consist of the four representative group waters. The NFC model does not produce a time history of seepage water chemistry. Instead, it produces four outputs, all of which are parametric, and which are combined only within the TSPA model when evaluating in-drift chemistry. The four outputs are:

- A set of EQ3/6 pickup files, used as initial seepage water compositions in the seepage evaporation abstraction. There are 132 files, representing four starting waters (selected to be representative of the 34 TSw water compositions believed to be representative of *in situ* ambient conditions at Yucca Mountain), three drift wall temperatures (30°C, 70°C, and 96°C), and 11 discrete values of water–rock interaction parameter (WRIP) (amount of feldspar dissolved).



027151DC\_164c.ai

Source: SAR Sections 2.3.5.3.4 and 2.3.5.5.4.

Figure 1. Flow Chart Illustrating How the Near-Field Chemistry Model and Seepage Evaporation Abstraction Are Integrated into the TSPA

- The WRIP map, which provides time histories for the WRIP value for seepage at 102 discrete time steps, for 336 different thermal histories at 20 different sequences of percolation flux values (four values, representing present-day, monsoonal, glacial-transition, and post-10,000-year climatic conditions), spanning the entire range used in the TSPA model.
- A beta distribution representing uncertainty in the WRIP value.
- A set of tables used to calculate the possible range of in-drift  $p\text{CO}_2$ . These tables are generated by extracting data from the EQ3/6 simulations used to make the EQ3/6 pickup files (bullet 1). They provide  $\text{CO}_2$  concentrations parametrically, as a function of representative water, drift wall temperature, and WRIP value.

**EQ3/6 Pickup Files** – The EQ3/6 pickup files are passed to the seepage evaporation abstraction, which uses them as starting files for the EQ3/6 seepage evaporation simulations. Each of the 132 files is used as the starting water composition for three EQ3/6 seepage evaporation simulations at  $10^{-2}$ ,  $10^{-3}$ , and  $10^{-4}$  bars, generating 396 seepage evaporation lookup tables, representing four starting waters, three waste package temperatures (30°C, 70°C, and 100°C; note that the 96°C pickup files are used to initialize the 100°C seepage evaporation simulations), 11 WRIP values, and three  $p\text{CO}_2$  values (SAR Section 2.3.5.5.4.2.1).

Prior to use in the EQ3/6 simulations that generate the pickup files, the initial pore-water compositions are pre-equilibrated to estimate missing components (e.g., aluminum, and pH,  $\text{HCO}_3^-$ , or  $\text{SiO}_2(\text{aq})$ ). This process is described in *Engineered Barrier System: Physical and Chemical Environment* (SNL 2007a, Section 6.3.2.3) and is not repeated here. The measured water compositions and the initial compositions used in the model are given in Table 1.

**WRIP Map** – The WRIP map is a direct feed to the TSPA model. It provides time histories of the WRIP value as a function of thermal history and percolation flux (SAR Section 2.3.5.3.4). The TSPA model selects a multiscale thermohydrologic model (MSTHM) (SNL 2008a) in-drift temperature-relative humidity history for realization of a waste package. The MSTHM history is associated with a sequence of percolation flux values corresponding to the four climate states. The TSPA model then calculates the thermal measure for the MSTHM simulation, which is the sum of the duration of drift wall boiling and the maximum drift wall temperature. It then selects the nearest matching thermal measure value in the WRIP table, and uses the percolation fluxes at each time step to interpolate between the columns on the WRIP map, which represent discrete percolation flux values. The result is a time history of WRIP values consistent with the MSTHM thermal history and percolation flux values.

**WRIP Uncertainty Distribution** – Uncertainty in the WRIP value is provided to the TSPA model as a beta distribution (SAR Section 2.3.5.3.4), with a mean, standard deviation, and maximum and minimum values. The uncertainty is largely due to uncertainty in the thermal history of the TSw tuff and its impact on the estimated ambient feldspar dissolution rate. Uncertainties in alteration mineral abundances and in the water–rock ratio are also incorporated. The derivation of the beta distribution is discussed in detail in the response to RAI: 3.2.2.1.3.3-004. The uncertainty is sampled as a multiplier on the nominal WRIP value

derived from the WRIP map at each time step; the multiplier is sampled only once per realization.

**In-Drift  $p\text{CO}_2$  Tables** – The set of tables used to calculate the possible range of in-drift  $p\text{CO}_2$  is also an input to the TSPA model. These tables are generated by extracting data from the EQ3/6 simulations used to make the EQ3/6 pickup files. They are used to calculate the possible  $\text{CO}_2$  range within the drift as a function of water group, drift wall temperature, and WRIP value. A description of the tables and their implementation is provided in *Engineered Barrier System: Physical and Chemical Environment* (SNL 2007a, Section 6.15.1). TSPA calculates a  $\text{CO}_2$  range at every time step, and then applies uncertainty by using a proportional offset within the range to select a single value. The offset is sampled once per realization.

### TSPA Implementation

For any given TSPA realization, the TSPA model randomly selects one of the four representative waters. Each of the waters is weighted equally (SAR Section 2.3.5.5.4.3), even though the representative group waters represent different numbers of pore-water analyses in each group. The model then selects a set of percolation fluxes (four values, representing present-day, monsoonal, glacial-transition, and post-10,000-year climatic conditions) and a thermal history for a representative waste package from the outputs of the MSTHM (SNL 2008a). The TSPA model uses the thermal measure (a metric representing the thermal history) to identify the most similar thermal history of the WRIP map to use, and uses the percolation fluxes to identify the appropriate columns at each time step (SAR Section 2.3.5.3.4). A time history of WRIP values is generated by interpolating between columns representing different percolation fluxes at each time step. Uncertainty in the WRIP value, due to uncertainty in the feldspar dissolution rate and water-rock ratio, is sampled once per realization, and implemented as a proportional offset on the nominal values derived from the WRIP map.

To calculate an in-drift water composition for a given time step, the TSPA model enters the WRIP map using a thermal measure and percolation flux set derived from the selected MSTHM simulation, and samples a preliminary WRIP value (SAR Section 2.3.5.5.4.3). Then, it applies uncertainty to the WRIP value to obtain a final WRIP value. This value is used, along with the representative water group and MSTHM-provided parameters (drift wall temperature, waste package temperature, and relative humidity), to estimate an in-drift  $p\text{CO}_2$  range from the NFC model  $\text{CO}_2$  tables. The  $p\text{CO}_2$  range is then sampled using an offset that is calculated once per realization to yield a single value for in-drift  $\text{CO}_2$  at each time step. Then, the TSPA model accesses the seepage evaporation abstraction lookup tables using the final WRIP value, the in-drift  $p\text{CO}_2$ , and the waste package temperature and relative humidity (both provided by the MSTHM model) to define the bounding lookup tables. Interpolation between tables is done using all four values to obtain specific concentration values for TSPA-relevant parameters ( $\text{Cl}^-$ ,  $\text{NO}_3^-$ ,  $\text{Cl}^-/\text{NO}_3^-$ , pH, and ionic strength).

Finally, uncertainties in individual chemical components provided to the TSPA model are added to the values extracted from the seepage evaporation abstraction lookup tables. The method of incorporating uncertainty and the magnitude of the uncertainty varies with the relative humidity

(SNL 2007a, Sections 6.12.3 and 6.15.1). For waters more dilute than the point of nitrate or chloride salt saturation, chloride and nitrate display very weak interactions with other species in solution, and are nearly interchangeable. As long as the sum of ( $\text{NO}_3^- + \text{Cl}^-$ ) is constant, the two individual component concentrations may vary widely without significantly affecting pH or other ion concentrations. For any single water group, nitrate and chloride can be partitioned using any nitrate-to-chloride ratio within the group, while holding the sum constant, without having any significant effect on other water components. At relative humidity values above that of salt separation,  $[\text{Cl}^-]$  and  $[\text{NO}_3^-]$  are sampled from the seepage evaporation tables, and the value ( $\text{NO}_3^- + \text{Cl}^-$ ) is calculated, and adjusted using uncertainties developed by *In-Drift Precipitates/Salts Model* (IDPS) (SNL 2007b). Then, the chloride-to-nitrate ratio is sampled from a discrete distribution of all the ratios within the selected water group. Finally,  $[\text{Cl}^-]$  and  $[\text{NO}_3^-]$  concentrations are back-calculated, using the value of  $[\text{NO}_3^- + \text{Cl}^- + \text{uncertainty}]$  and the selected  $\text{Cl}^-/\text{NO}_3^-$  value. The value of  $\text{Cl}^-/\text{NO}_3^-$  is sampled by TSPA only once per realization, when the water group is selected. At relative humidity values below that of salt saturation, IDPS uncertainties in  $[\text{Cl}^-]$ ,  $[\text{NO}_3^-]$ , and  $\text{Cl}^-/\text{NO}_3^-$  are implemented directly.

Uncertainty in pH is implemented in a similar fashion, by sampling a discrete distribution of uncertainties, based on the comparisons between IDPS model predictions and measured data, at relative humidity values above that of salt precipitation, and by implementing IDPS uncertainties directly at lower relative humidity values (SNL 2007a, Section 6.12.3). IDPS uncertainties in ionic strength are implemented at all relative humidity values.

### **Propagation of Variability and Uncertainty**

The NFC model and seepage evaporation abstraction are closely linked, and uncertainty in in-drift water compositions is accommodated by sampling parameter uncertainties in both models, and also by epistemic sampling of externally derived parameter values (e.g., MSTHM thermal histories and percolation flux ranges) in the TSPA model. Within the NFC model, variability in pore-water compositions is incorporated by the use of the four representative waters to represent the 34 screened-in waters. Also implemented in this model is an uncertainty distribution in the WRIP value. The WRIP uncertainty distribution is, in turn, based on estimates of uncertainty in the ambient feldspar dissolution rate and in hydrologic properties determining the water-rock ratio (SAR Section 2.3.5.3.3.4). The derivation of the WRIP uncertainty distribution is described in detail in the response to RAI: 3.2.2.1.3.3-004. Variability in thermal histories is accommodated in the NFC model by use of 336 different thermal histories, representing three different rock thermal conductivities and 112 different locations within the repository, and variability in percolation flux by use of 20 different sequences of percolation flux, covering the range used in the TSPA model. Finally, uncertainty in the in-drift  $p\text{CO}_2$  is incorporated by sampling from a range of values at any given time step.

Within the seepage evaporation abstraction, variability in starting water composition is propagated from the NFC model in the EQ3/6 pickup files for the four representative waters. Following sampling of the seepage evaporation lookup tables, additional starting water uncertainty is incorporated by sampling the  $\text{Cl}^-:\text{NO}_3^-$  ratios for all 34 pore waters (SAR

Section 2.3.5.5.4.3). Finally, uncertainties in the IDPS process model are incorporated by application of IDPS uncertainties to individual parameter values.

### 1.3. AMBIENT WATER COMPOSITIONS PREDICTED BY THE NEAR-FIELD CHEMISTRY MODEL

Prior to use in the EQ3/6 simulations which generate the pickup files, the initial pore-water compositions are pre-equilibrated to estimate missing components (e.g., aluminum, and pH,  $\text{HCO}_3^-$ , or  $\text{SiO}_2(\text{aq})$ ) (SNL 2007a, Section 6.3.2.3). The measured water compositions and the initial pre-equilibrated compositions used in the model are given in Table 1. The pore waters are equilibrated with a  $p\text{CO}_2$  of  $10^{-3}$  bars, the assumed value for in situ ambient  $\text{CO}_2$  concentrations in the TSw (SNL 2007a, Section 7.1.2.2). This generates a bicarbonate concentration for water ESF-HD-PERM-3/34.8-35.1 and a pH value for ESF-HD-PERM-3/56.7-57.1/UC. It also results in shifts in  $\text{Ca}^{2+}$  and  $\text{HCO}_3^-$  concentrations and pH for most of the waters, which appear to have equilibrated at a slightly higher  $p\text{CO}_2$  ( $\text{Ca}^{2+}$  and  $\text{HCO}_3^-$  both decrease upon equilibration), probably due to minor amounts of microbial activity during core storage. A  $\text{SiO}_2(\text{aq})$  concentration is calculated for pore water ESF-HD-PERM-3/56.7-57.1/UC by equilibrating with  $\text{SiO}_2(\text{am})$ . Aluminum concentrations are estimated for all samples by first assuming equilibrium with alkali feldspar, resulting in supersaturation with several secondary aluminosilicates, and then in a second simulation, allowing the Al-solubility-limiting phase to precipitate. Stellerite is the solubility-limiting phase for Al for all four waters. The amount of stellerite that precipitates is too small to significantly affect solution concentrations for any other aqueous species.

Table 1. Measured and Pre-equilibrated Compositions for the Representative Group Waters

Pore Water ID	SD-9/1184.7-1184.8/UC		ESF-THERMALK-017/26.5-26.9/UC		ESF-HD-PERM-3/34.8-35.1		ESF-HD-PERM-3/56.7-57.1/UC*	
	1		2		3		4	
	Meas.	Equil.	Meas.	Equil.	Meas.	Equil.	Meas.	Equil.
pH	8.2	8.10	7.7	7.85	8.31	7.83	—	7.91
Na (mg/L)	59	59	45	45	62	62	123	122
K (mg/L)	4.8	4.8	14.4	14.4	9	9	13.8	13.7
Mg (mg/L)	0.7	0.7	7.9	7.9	17.4	17.4	16.7	16.6
Ca (mg/L)	19	16	62	54	97	61	59.9	44
Cl (mg/L)	23	23	67	67	123	123	146	146
SO <sub>4</sub> (mg/L)	16	16	82	82	120	120	126	126
HCO <sub>3</sub> (mg/L)	142	133	126	78	—	77	149	91
NO <sub>3</sub> (mg/L)	16	16	44	44	10	10	57.4	57.4
F (mg/L)	2.2	2.2	1.4	1.4	0.76	0.76	1.3	1.3
SiO <sub>2</sub> (mg/L)	42	42	52	52	75	75	—	111
Equil. $p\text{CO}_2$	-3.06	-3.0	-2.64	-3.0	—	-3.0	—	-3.0

\* Na, K, and Mg concentrations differ slightly for measured and equilibrated values because of minor changes in the reported values between the preliminary measured values, used in the EQ3/6 equilibration calculations, and the final, qualified values.

In the next step, when the EQ6 simulations used to create the pickup files used by the seepage evaporation abstraction are run, calcite and amorphous silica are titrated into each water in excess, in addition to fixed amounts of alkali feldspar. For conditions representing ambient (e.g., at 23°C with no feldspar added), this titration step has no effect on the  $\text{Ca}^{2+}$  and  $\text{HCO}_3^-$  concentrations, as the four waters are all saturated with respect to calcite after the equilibration step at a  $p\text{CO}_2$  of  $10^{-3}$  bars, but increases the  $\text{SiO}_2(\text{aq})$  concentrations to about 110 mg/L in all four waters. Justification for using amorphous silica as the solubility-limiting phase for  $\text{SiO}_2(\text{aq})$  is provided in *Engineered Barrier System: Physical and Chemical Environment* (SNL 2007a, Section 6.3.2.4.1).

The NFC model does not explicitly predict seepage compositions; instead, it predicts the amount of water–rock interaction. Because waters from the repository level, which have already been modified by water–rock interactions, are used as starting waters, the model is designed to predict no additional water–rock interaction under ambient conditions. Also, uncertainties in individual chemical component concentrations are implemented later, in the seepage evaporation abstraction. Therefore, the four equilibrium compositions in Table 1 (with the exception that all  $\text{SiO}_2(\text{aq})$  values would be around 110 mg/L) would be predicted. It is more informative to examine the results of the seepage evaporation abstraction at ambient or near-ambient values, as these include uncertainties in each parameter. To do this, results have been extracted from localized corrosion initiation analysis performed for the TSPA and are presented below. As described in the response to RAI: 3.2.2.1.3.3-017, equivalent results could be obtained from the TSPA model. The values represent predicted in-drift chemistry at 1,000,000 years, for percolation subregion 5 (differences between subregions are minor). To keep the amount of data manageable, only the data for 100 randomly selected locations are shown. The compositional data are plotted as a function of relative humidity because even after ambient or near-ambient conditions have been achieved, minor variations in in-drift relative humidity result in large changes in pH and water composition. Select results are discussed below, and in the response to RAI: 3.2.2.1.3.3-017, which also provides additional information on how the data were compiled. The results presented below include plots of the 34 pore-water compositions relative to the ranges of in-drift chemistries predicted by the TSPA model. The seepage evaporation abstraction does not predict seepage chemistry but rather in-drift chemistry; the evaporating in-drift waters are treated as not being in contact with the rock. Hence, the range of seepage evaporation abstraction results differs slightly from the pore-water range, but the ranges are similar.

Predicted calcium concentrations at ambient or near-ambient conditions are not provided in this response because the localized corrosion initiation analysis does not calculate calcium concentrations. However, a modified version of the localized corrosion initiation analysis, which does include calcium, is used in the response to RAI: 3.2.2.1.3.3-009 to estimate in-drift water compositions from repository closure to 1,000,000 years. Predicted calcium concentrations are provided graphically in that RAI.

## pH Ranges

Figure 2(a) shows predicted pH conditions at the surface of commercial spent nuclear fuel (SNF) waste packages in Percolation Subregion 5 as a function of relative humidity (RH) at  $t = 1,000,000$  years given by the localized corrosion initiation analysis for the TSPA. Small changes in relative humidity result in large changes in evaporative concentration, so a large range of pH values is predicted. Figure 2(b) plots the pH of the 34 pore waters as a function of relative humidity, which is equal to the activity of water in the pore-water solutions. At relative humidity values higher than that representing equilibrium with the starting waters, the water compositions are diluted relative to the starting waters; pH values in this relative humidity range evolve to lower values, towards pure water in equilibrium with a  $p\text{CO}_2$  of  $10^{-3}$  bars. At relative humidities lower than that representing equilibrium with the initial pore waters, the waters are evaporatively concentrated, and the trends in pH vary with the starting water. The pH values for Group 1 water increase significantly with minor decreases in relative humidity, while for Group 2, 3, and 4 waters, pH decreases slightly relative to the starting waters. Overall, the pH range is approximately 7.4 to 9.6 at ambient conditions. (Note that on Figure 2 and on following plots, water “types” are equivalent to water “groups.”)

The solid lines in Figures 2(a) and 2(b) represent the water compositions extracted from the seepage evaporation abstraction lookup tables for “ambient” conditions, corresponding to  $T = 30^\circ\text{C}$ ,  $p\text{CO}_2 = 10^{-3}$  bars, and  $\text{WRIP} = 0$ , since the lookup tables are discretized with respect to temperature, and at values below  $30^\circ\text{C}$ , the  $30^\circ\text{C}$  compositions are used. Also shown is the seepage evaporation abstraction uncertainty range. Dashed lines in Figures 2(a) and 2(b) are the lower bounds, while double-dotted dashed lines are the upper bounds of pH for each of the four representative waters upon dilution or evaporation. Since the relative humidity at near-ambient conditions is above that of salt saturation, the uncertainty in pH is defined by sampling a discrete distribution of values (SNL 2007a, Section 6.12.3) derived from IDPS model validation comparisons. The figures show that the localized corrosion initiation analysis results fall within the upper and lower bounds defining the uncertainty range of the seepage evaporation abstraction, and also that the 34 initial seepage water compositions are captured within the uncertainty range.

## Range of Chloride-to-Nitrate Ratios

Figures 3(a) and 3(b) show chloride-to-nitrate concentration ratios (mol/mol) at the surface of commercial SNF waste packages in Percolation Subregion 5 as a function of relative humidity at  $t = 1,000,000$  years given by the localized corrosion initiation analysis, and the pore-water chloride-to-nitrate concentration ratios, respectively. Over the range of relative humidities shown, no salts precipitate, so chloride and nitrate simply concentrate/dilute in evaporating/condensing solutions; the chloride-to-nitrate ratio is therefore independent of relative humidity and is sampled for each group from a discrete distribution of the ratios of each water in the group (Section 1.2 and Figure 1). The range of chloride-to-nitrate ratios for each group is as follows: Group 1, 0.783 to 6.121; Group 2, 2.359 to 3.187; Group 3, 9.778 to 64.128; and Group 4, 4.448 to 8.212. Because the uncertainty in the chloride-to-nitrate ratios is incorporated by sampling discrete distributions for each water group, the 34 initial seepage water

compositions are captured within the uncertainty range, and the upper and lower bounds for each water group correspond to individual pore-water values.

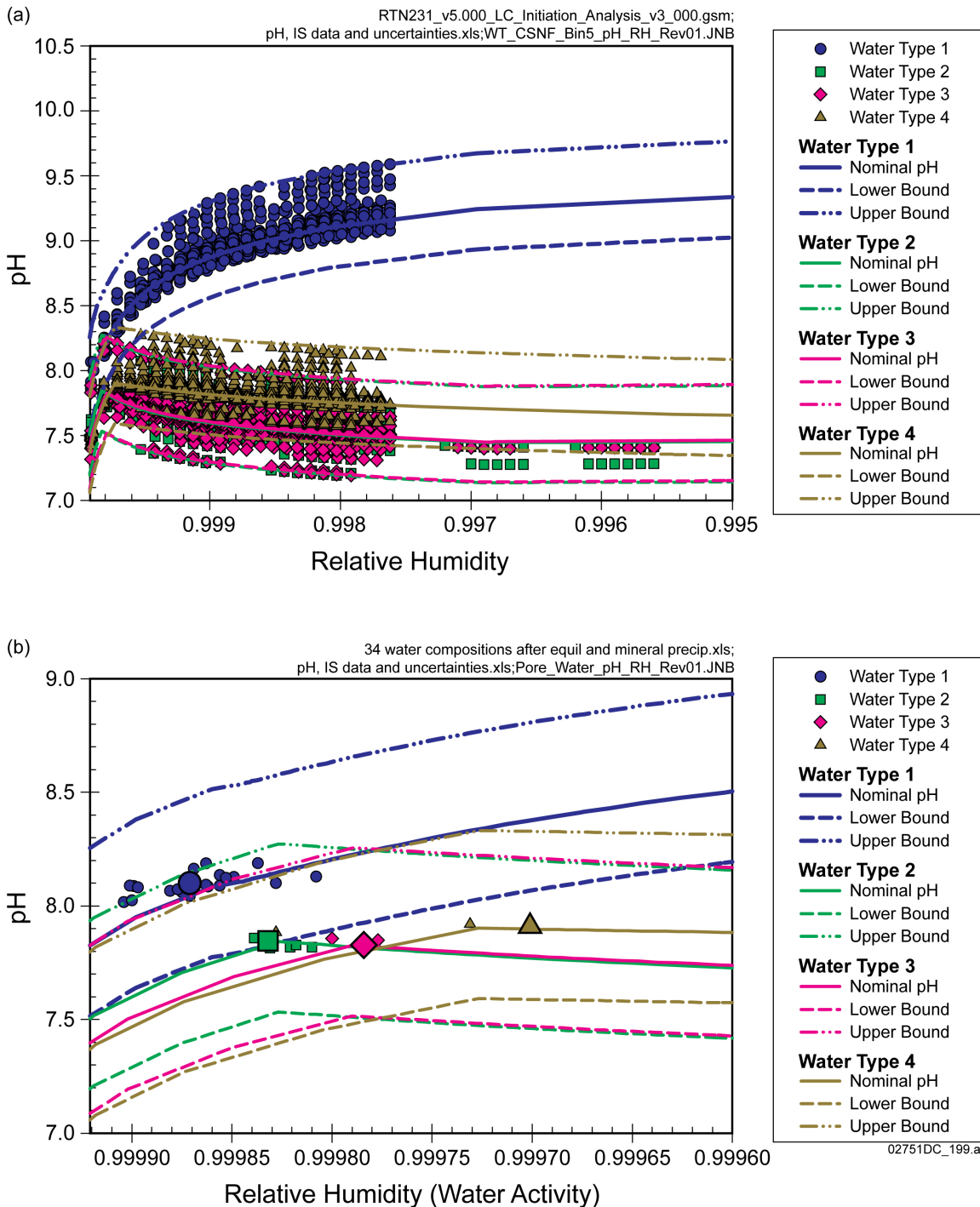


Figure 2. Comparison of In-drift Seepage Evaporation Abstraction Uncertainty Ranges to (a) TSPA Model Results for pH Conditions at the Surface of Commercial SNF Waste Packages in Percolation Subregion 5 as a Function of RH at  $t = 1,000,000$  Years; and (b) Pore Water Compositions (larger symbols indicate representative waters)

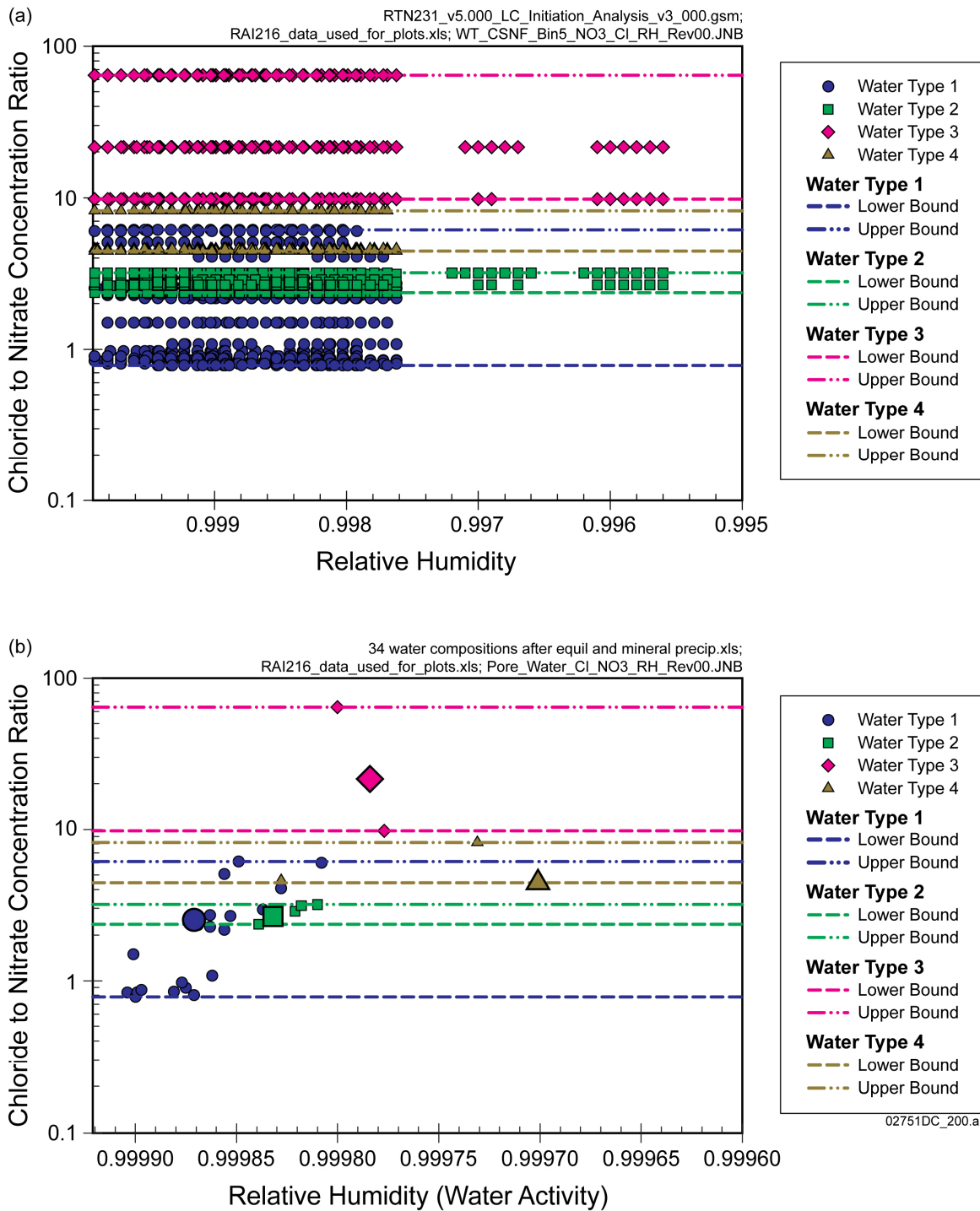


Figure 3. Comparison of In-drift Seepage Evaporation Abstraction Uncertainty Ranges to (a) TSPA Model Results for Chloride-to-Nitrate Concentration Ratio (mol/mol) at the Surface of Commercial SNF Waste Packages in Percolation Subregion 5 as a Function of RH at  $t = 1,000,000$  Years; and (b) Pore Water Compositions (larger symbols indicate representative waters)

### **Range of Chloride and Nitrate Concentrations**

Figures 4(a) and 5(a) show chloride and nitrate concentrations (mol/kg), respectively, at the surface of commercial SNF waste packages in Percolation Subregion 5 as a function of RH at  $t = 1,000,000$  years, given by the localized corrosion initiation analysis. The figures show that the localized corrosion initiation analysis results fall within the uncertainty range of seepage evaporation abstraction outputs. Figures 4(b) and 5(b) compare chloride and nitrate concentrations in the pore waters to the uncertainty ranges from the seepage evaporation abstraction; most of the 34 initial seepage water compositions fall within the ranges, but a few of the Group 1 waters fall outside the predicted ranges. Several factors associated with alkalinity may contribute to this, because bicarbonate comprises over half the anion normality in Group 1 waters, and the relative humidity controls the total ionic strength as opposed to the chloride or nitrate concentration. As dilution goes to infinity, the chloride concentration goes to zero, but the ionic strength does not, because equilibrium with atmospheric  $\text{CO}_2$  maintains measurable carbonate concentrations in solution. Slight differences in pore-water composition result in differing degrees of carbonate buffering and slightly different trends in relative humidity with increasing dilution. Hence, as the representative waters are diluted, they do not necessarily evolve along a track that intersects the other pore waters, especially the most dilute ones. Moreover, use of the  $30^\circ\text{C}$  lookup tables to represent ambient temperatures ( $\sim 23^\circ\text{C}$ ) results in small errors in predicted bicarbonate concentration, once again, affecting the relative humidity trend with increasing dilution. Finally, the seepage evaporation abstraction assumes that the water is not in contact with minerals in the rock, and hence does not predict the exact conditions represented by the pore waters. Although the seepage evaporation abstraction does not bound the pore-water ranges of chloride and nitrate at very low relative humidity, this has no effect on TSPA calculations, because the dilute ambient and near-ambient waters are benign with respect to localized corrosion of Alloy 22 (SNL 2008b, Appendix O).

### **Range of Ionic Strength**

Figure 6(a) shows ionic strengths at the surface of commercial SNF waste packages in Percolation Subregion 5 as a function of RH at  $t = 1,000,000$  years given by the localized corrosion initiation analysis, and Figure 6(b) compares the ionic strengths of the pore waters to the uncertainty range of the seepage evaporation abstraction. Once again, the figures show that the localized corrosion initiation analysis results fall within the uncertainty range of seepage evaporation abstraction outputs, and also that the variability in the 34 initial seepage water ionic strengths is captured within the uncertainty range of the abstraction.

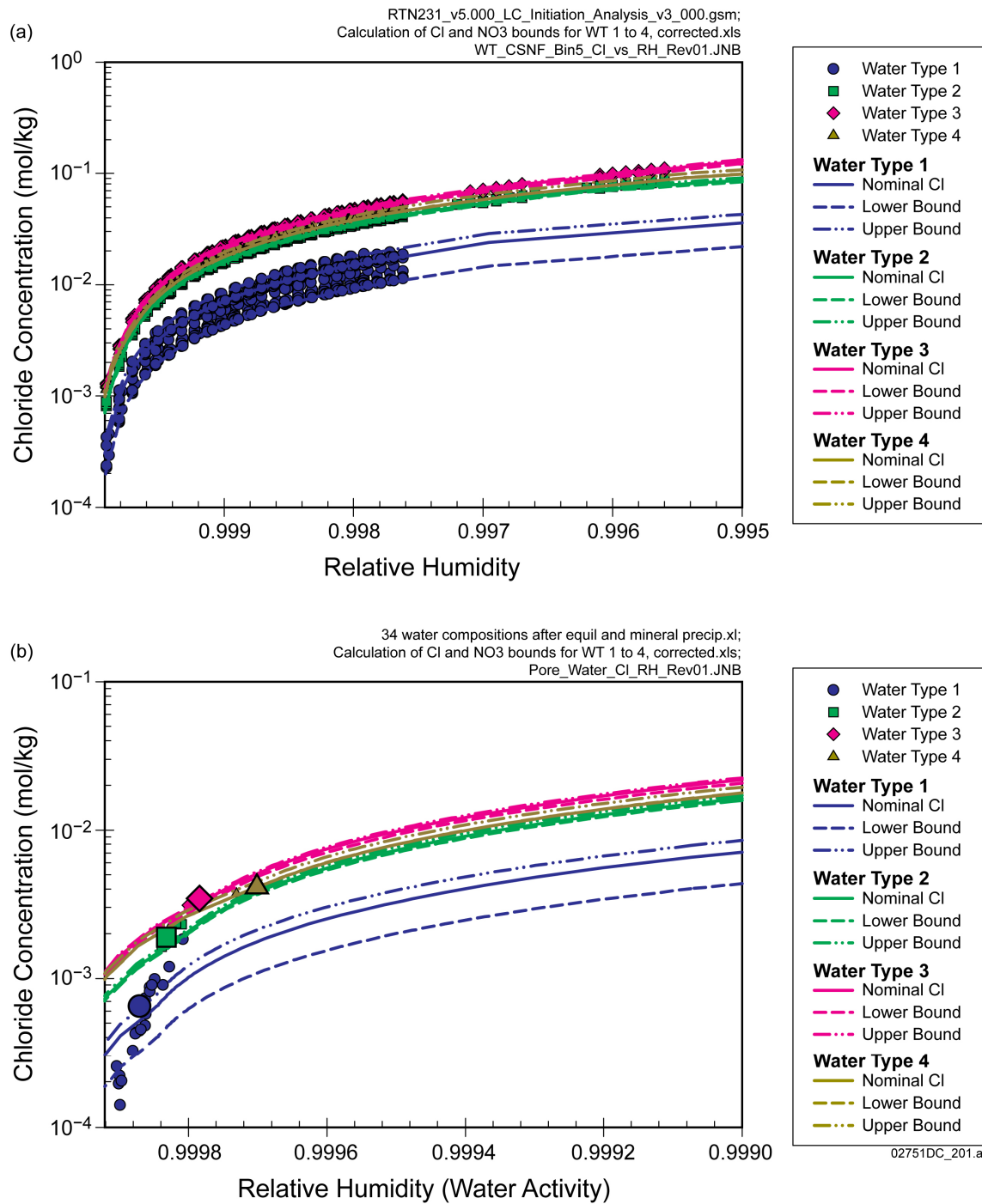


Figure 4. Comparison of In-drift Seepage Evaporation Abstraction Uncertainty Ranges to (a) TSPA Model Results for Chloride Concentrations (mol/kg) at the Surface of Commercial SNF Waste Packages in Percolation Subregion 5 as a Function of RH at  $t = 1,000,000$  Years; and (b) Pore Water Compositions (larger symbols indicate representative waters)

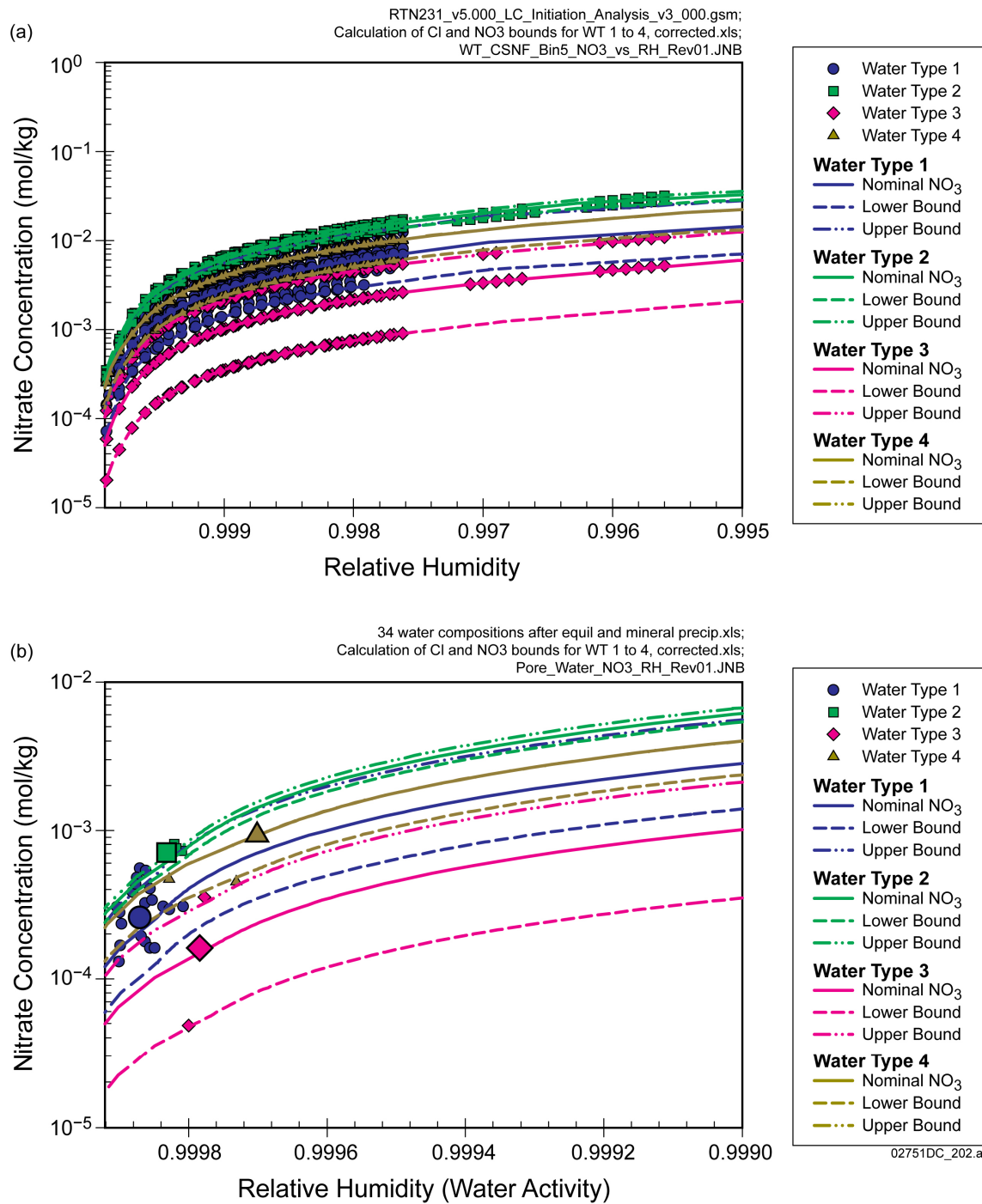


Figure 5. Comparison of In-drift Seepage Evaporation Abstraction Uncertainty Ranges to (a) TSPA Model Results for NO<sub>3</sub> Concentrations (mol/kg) at the Surface of Commercial SNF Waste Packages in Percolation Subregion 5 as a Function of RH at t = 1,000,000 Years; and (b) Pore Water Compositions (larger symbols indicate representative waters)

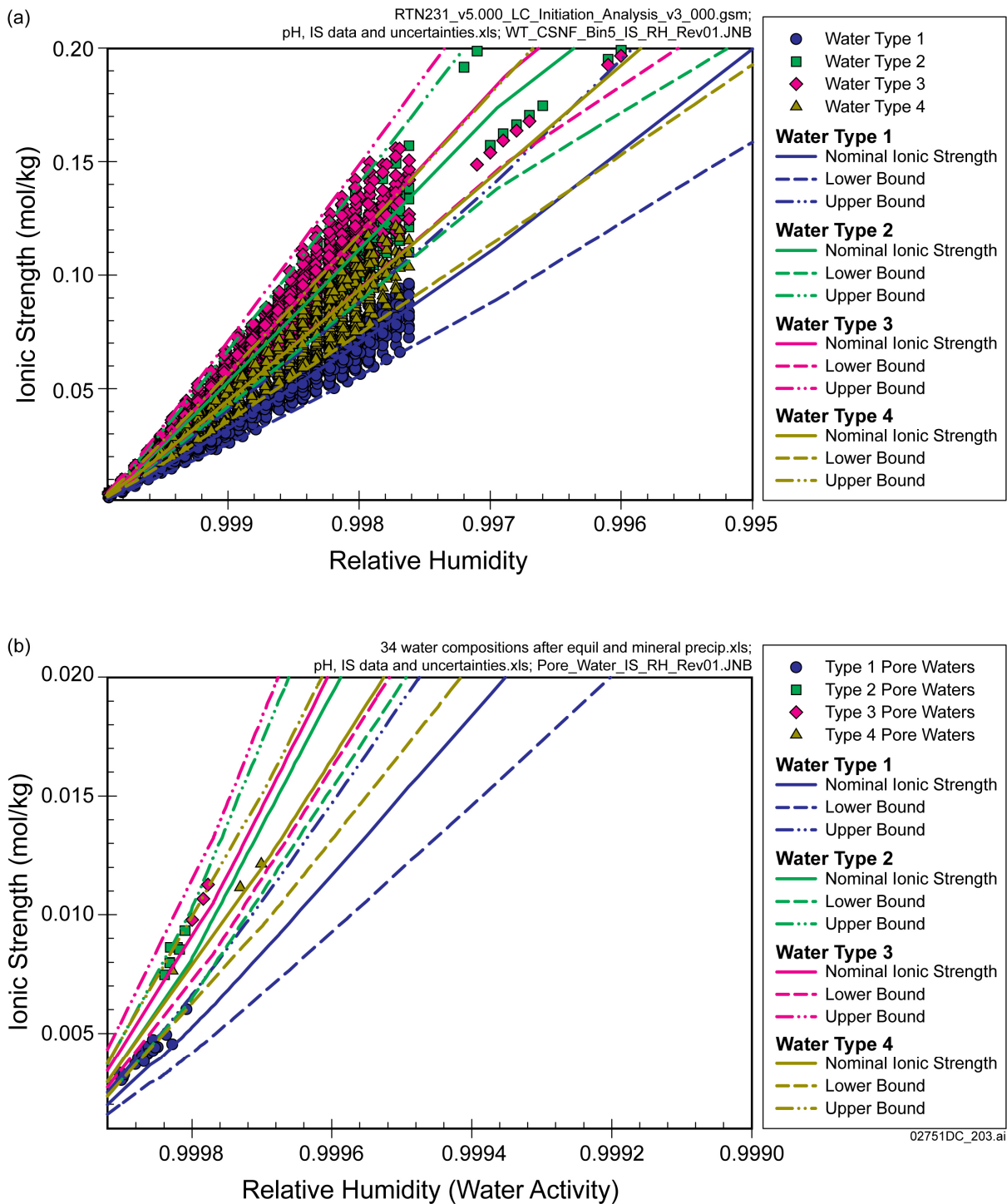


Figure 6. Comparison of In-drift Seepage Evaporation Abstraction Uncertainty Ranges to (a) TSPA Model Results for Ionic Strengths at the Surface of Commercial SNF Waste Packages in Percolation Subregion 5 as a Function of RH at  $t = 1,000,000$  Years; and (b) Pore Water Compositions (larger symbols indicate representative waters)

**Range of In-Drift  $p\text{CO}_2$**

Figure 7 shows in-drift  $p\text{CO}_2$  concentrations (bars) for commercial SNF waste packages in Percolation Subregion 5 as a function of relative humidity at  $t = 1,000,000$  years given by the localized corrosion analysis. The figure shows that even at very long times, there is a slight variation in predicted  $p\text{CO}_2$  values, especially for Group 1 waters. The plot of the initial 34 pore waters is not included here, as all pore waters were equilibrated at  $10^{-3}$  bars and would plot at that value.

As can be seen from Figures 2 through 6, predicted in-drift water compositions cover a wide range of compositions and concentrations due to minor variations in in-drift relative humidity. The predicted range encompasses the observed pore-water compositions.

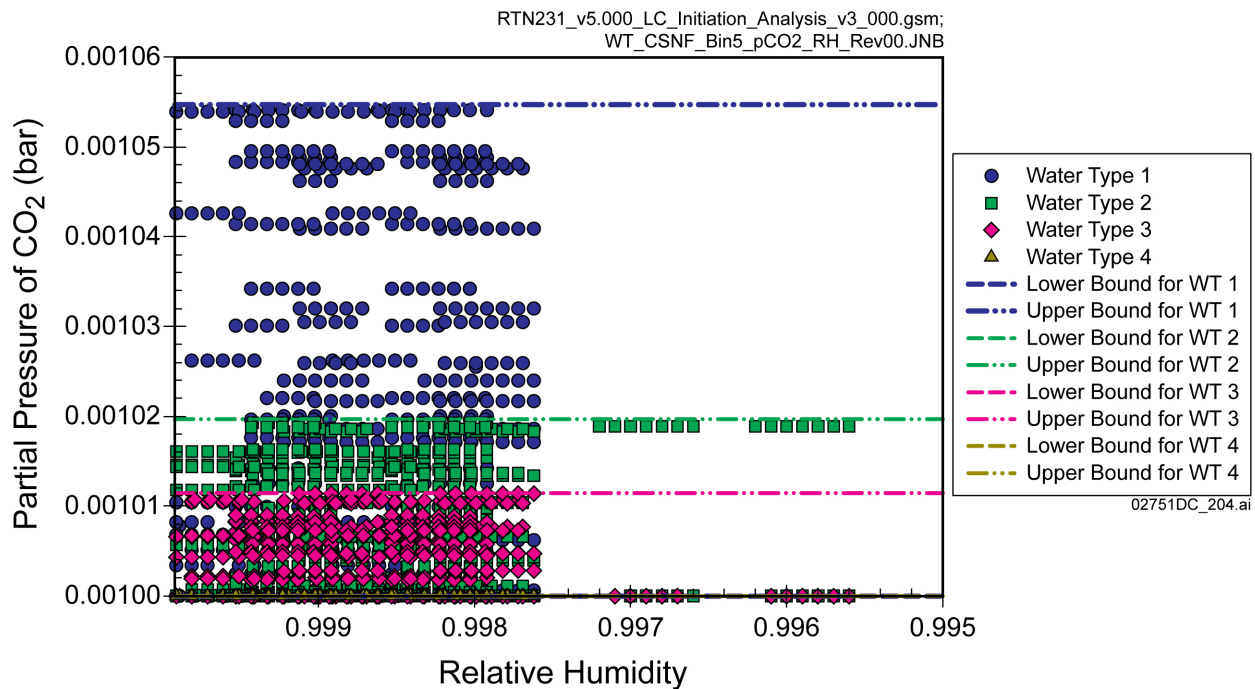


Figure 7. Comparison of Near Field Chemistry Model Uncertainty Ranges to (a) TSPA Model Results for In-Drift  $p\text{CO}_2$  Values at the Surface of Commercial SNF Waste Packages in Percolation Subregion 5 as a Function of RH at  $t = 1,000,000$  Years

#### **1.4 POTENTIAL USE OF THE THC SEEPAGE MODEL AS AN ALTERNATIVE CONCEPTUAL MODEL IN THE TSPA**

The THC seepage model and the NFC model are not alternative conceptual models that can be comparably implemented in TSPA. Each is developed and used for different purposes in supporting the license application. The THC seepage model produces a suite of water chemistry compositions conditioned to specific thermal histories and percolation flux histories. As explained in Section 1.2 of this response, the NFC model determines the extent of water–rock interaction for seepage water, which is combined with other TSPA submodel results to represent water chemistry in the drift. Because the THC seepage model is primarily used to evaluate thermally driven coupled processes for FEP screening, the treatment of uncertainty and variability can be limited while adequately accomplishing this function. For determination of seepage water chemistry in the TSPA model, more detailed representation of parameter uncertainty and variability is used in the NFC model and the related submodels.

The THC seepage model is a fully coupled thermal-hydrologic-chemical reactive transport simulation (SAR Section 2.3.5.2.3; SNL 2007c) that is used for evaluating the consequences of THC processes in support of FEP screening. The current revision of the THC seepage model consists of eight simulations, two with each of the four group waters. The THC seepage model simulates thermal histories at two locations in the repository, corresponding to generic “center” and “edge” locations, and uses a single set of host-rock thermal conductivity values (SNL 2007c, Section 6.5.5.4). All eight simulations are run using a single set of three percolation fluxes representing the mean values for the 30th percentile infiltration map for the present-day, monsoonal, and glacial-transition climatic conditions (SAR Section 2.3.5.2.3); the glacial-transition percolation flux was also used to represent post-10,000-year climatic conditions. The “center” and “edge” simulations carried out by the THC seepage model are sufficient to evaluate the major effects of THC processes for FEP screening, but do not provide sufficient discretization to represent the wider range of potential seepage water compositions in the repository at any given point in time.

In contrast, the NFC model and the related TSPA submodels that determine in-drift water chemistry capture uncertainty in modern and future percolation fluxes, in host-rock thermal conductivity, and in water–rock interaction parameters. The approach uses the same sampled values for percolation flux and thermal conductivity as are used in other parts of the TSPA model that represent waste package and waste form degradation, and radionuclide transport. For any given climate state, the range of percolation flux implemented in the TSPA and in the MSTHM covers more than two orders of magnitude (SNL 2007a, Table 6.3-1). Since percolation flux is directly related to transport time, the corresponding range in the extent of water–rock interaction (represented by the NFC model) is approximately two orders of magnitude. In addition, the MSTHM generates thermal histories for thousands of waste package locations throughout the repository footprint, calculated for the full range of percolation flux uncertainty and variability, and for the range of host-rock thermal conductivity values. The resulting range of temperature and relative humidity behaviors is much greater than could be used in the THC seepage model.

The NFC model also incorporates significant uncertainty in the ambient feldspar dissolution rate by sampling a range of values covering about a factor of 14 (SNL 2007a, Section 6.12.2.5). The range of feldspar dissolution rates used in the NFC model is derived from site-specific data, calculated from the amount of secondary aluminosilicates present, and adjusted for the early thermal history of the tuff (see response to RAI: 3.2.2.1.3.3-004).

### **Comparison with the Ambient Feldspar Dissolution Rate and Activation Energy Used in the THC Seepage Model**

The basis of the RAI suggests that the ambient feldspar dissolution rate and  $E_a$  used by the THC seepage model might constitute an alternative conceptual model. The following discussion describes why the treatment of these parameters in the NFC model is more appropriate for application in the TSPA.

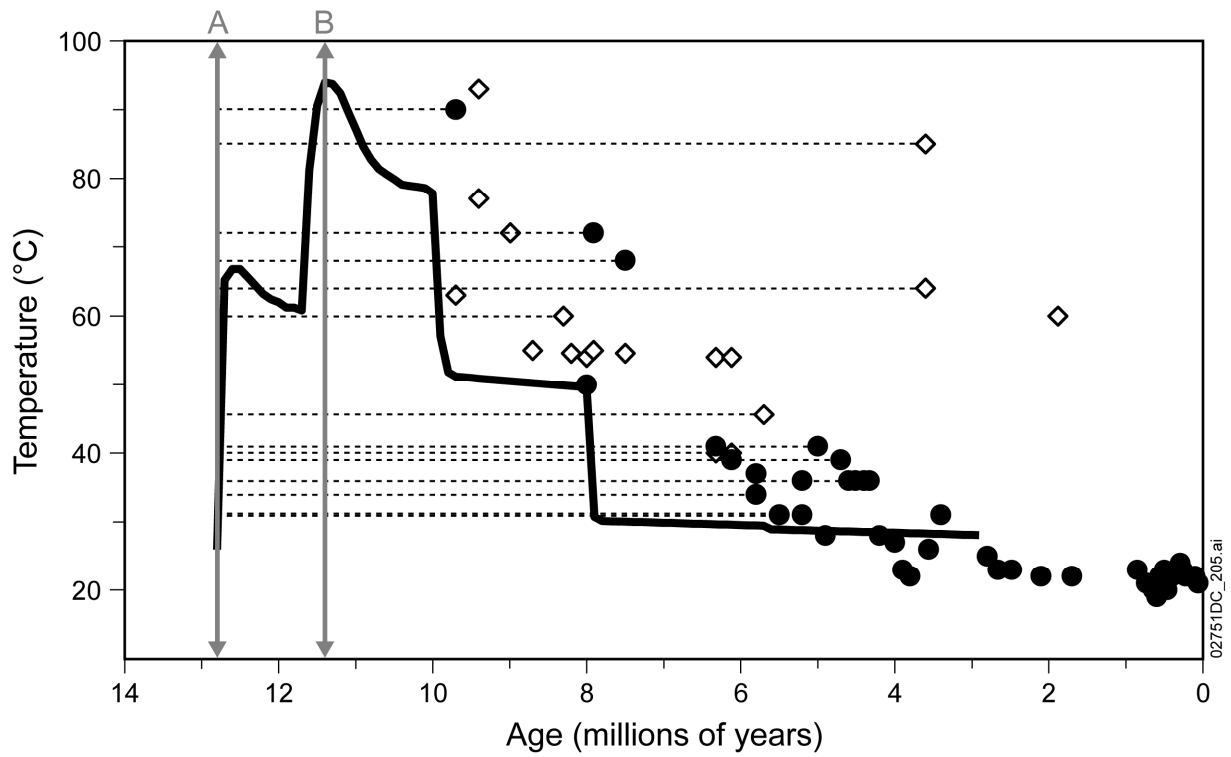
The THC seepage model uses an alkali feldspar dissolution rate based on laboratory experiments which is decreased by a factor of 10,000 to account for the observation that field-based rates are commonly slower than laboratory-measured dissolution rates (SNL 2007c, Section H.3.3). The  $E_a$  for feldspar dissolution used in the THC seepage model is from a different published source (SNL 2007c, Section 4.1.7).

The NFC model uses site-specific data—the abundance of secondary aluminosilicate minerals in the rock—to calculate the amount of feldspar dissolved (assuming Al is conserved) since the eruption of the tuff. The resulting average feldspar dissolution rate is  $5.94 \times 10^{-9}$  mol/yr per kg tuff. However, the tuff underwent an extended thermal pulse early in the history of the unit, and only cooled to ambient temperatures about 5 million years ago. Because the feldspar dissolution rate is a function of temperature, this means that the ambient temperature (23.4°C) feldspar dissolution rate cannot be equal to the rate averaged over the age of the tuff. Petrographic studies show that this is true—most of the alteration occurred early in the history of the tuff (SNL 2007a, Section 6.12.2). The feldspar dissolution rate used in the NFC model is calculated from the total observed amount of feldspar dissolution (as represented by secondary alteration minerals), using an assumed  $E_a$  value of 49 kJ/mol to correct for the thermal history of the tuff. This calculation uses a bounding approach and provides a distribution for the ambient feldspar dissolution rate (see response to RAI: 3.2.2.1.3.3-004) covering a range from  $3.14 \times 10^{-9}$  mol/yr per kg tuff to  $4.07 \times 10^{-10}$  mol/yr per kg tuff. In contrast, the THC seepage model uses an ambient rate that is equivalent to  $1.27 \times 10^{-8}$  mol/yr per kg tuff.

The THC seepage model thus uses more limited information to estimate the ambient feldspar dissolution rate than the NFC model. This results in a slight over-prediction of feldspar dissolution by the THC model, which is not significant with respect to the use of the THC model for FEP screening. The FEPs for which the THC model is used mainly deal with the effects of dryout and re-dissolution of salts around the drift on seepage chemistry, the effects of mineral precipitation on hydrologic properties of the host rock, and the effects of near-field chemical processes on radionuclide transport. The slight over-prediction of feldspar dissolution during the thermal pulse has little effect on these processes because the rate is still slow, and the thermal pulse is short.

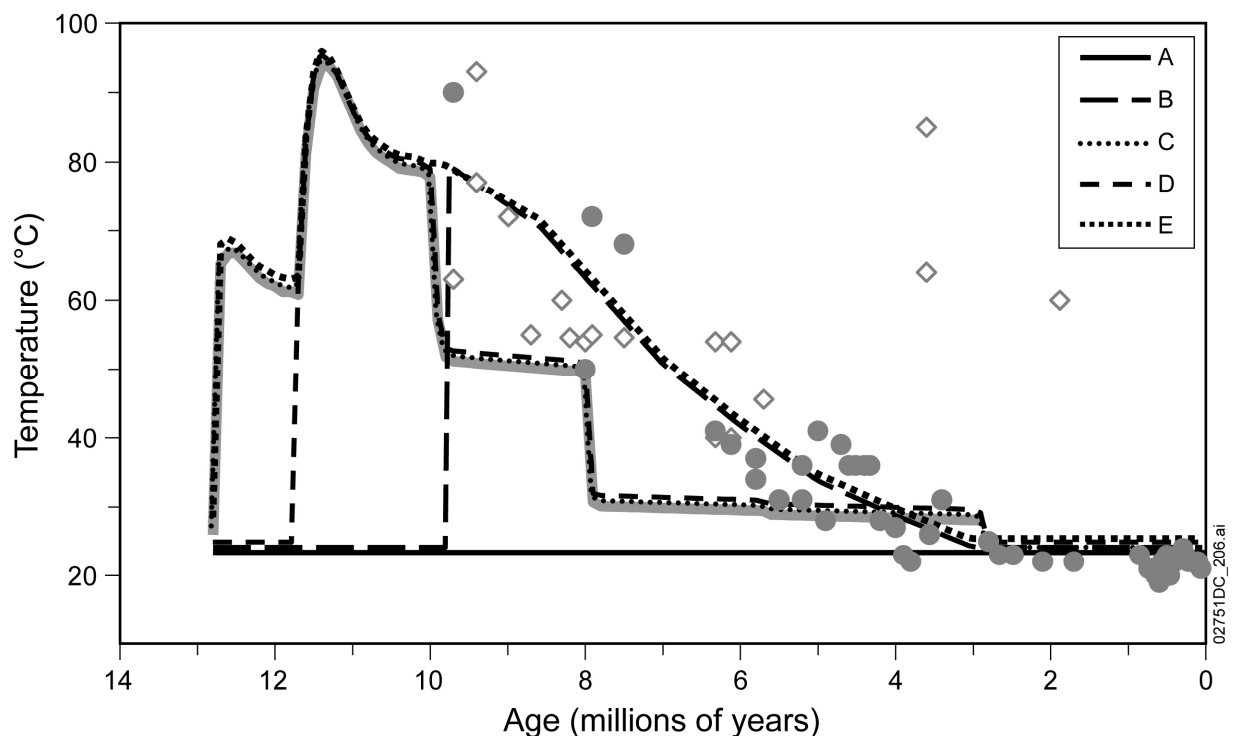
Because the NFC model feldspar dissolution rate is calibrated to the thermal history of the tuff using a specific  $E_a$ , the parameters cannot co-vary (see the response to RAI: 3.2.2.1.3.3-004). The same extent of alteration would be calculated using a faster alteration rate and a lower  $E_a$ , or a slower rate and a higher  $E_a$ . To further support the estimated range used for the NFC model, this response presents a new calculation that is similar to, but more detailed than, the calculation used in the model report to calculate the uncertainty in the feldspar dissolution rate (SNL 2007a, Section 6.12.2). In this approach, specific thermal histories for the tuff are developed and subdivided into time steps, for calculating the cumulative amount of feldspar dissolved, to compare with the accumulated abundance of secondary aluminosilicates (approximately 3.4% of the original feldspar has dissolved; SNL 2007a, Table 4.1-9 and Section 6.3.2.4.2). The calculation is repeated for different ambient feldspar dissolution rates and  $E_a$  values, and for several candidate thermal histories which are based on thermochronologic measurements on fracture minerals from Yucca Mountain (Figure 8), and on modeled thermal histories developed for the TSw tuff by the U.S. Geological Survey (USGS). The following possible thermal histories were used in the calculations (Figure 9):

- (A) No thermal pulse; 12.8 Ma of ambient temperatures (23.4°C). This yields the largest estimate for the ambient feldspar dissolution rate, but is inconsistent with the thermal history of the tuff.
- (B) The thermal history based on thermochronologic measurements, with ambient temperatures assumed prior to 9.8 Ma. This approach probably underestimates the duration of elevated temperatures in the thermal history and overestimates the ambient feldspar dissolution rate.
- (C) The thermal history proposed by the USGS for a depth of 200 meters.
- (D) The thermal history proposed by the USGS for a depth of 200 meters, assuming ambient temperatures prior to 11.6 Ma. This scenario accounts for the fact that the earlier thermal history is not well constrained.
- (E) The thermal history based on thermochronologic measurements, but applying the history proposed by the USGS for a depth of 200 meters, prior to 9.8 Ma.



NOTE: Open symbols represent fluid inclusion temperatures; closed symbols are  $\delta^{18}\text{O}$  values in calcite. Ages are  $^{207}\text{Pb}/^{235}\text{U}$  ages of chalcedony or opal associated with the calcite. If data represent minimum ages for calcite deposition, tie lines connect the measured age to the eruptive age of the Topopah Spring Tuff. The solid line represents the thermal model (for a depth of 200 m) proposed by the USGS. Points A and B represent the Eruptive age of the Paintbrush Group eruptions and the Timber Mountain Group Eruptions, respectively.

Figure 8. Thermochronologic Data from Fracture Minerals in the Topopah Spring Tuff



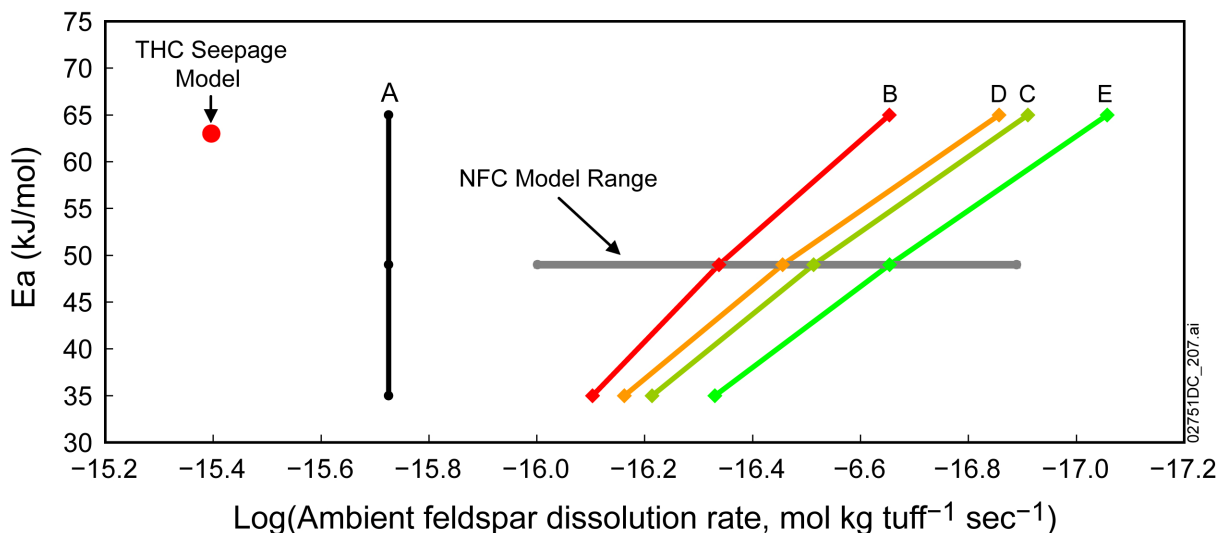
NOTE: Data points and thermal model (gray) are from Figure 8.

Figure 9. Possible TSw Thermal Histories (A through E) Used to Evaluate the Possible Range of Ambient Feldspar Dissolution Rates and  $E_a$  Values

For each of the possible thermal histories, the cumulative amount of feldspar dissolved is integrated through time, using the  $E_a$  to adjust the dissolution rate from the ambient value for each time interval. The combinations of ambient dissolution rate and  $E_a$  values that reproduce the average observed cumulative feldspar dissolution are calculated for histories A through E. The results of these calculations are summarized in Figure 10. The lines A to E represent the possible thermal histories discussed above; in each case, ambient feldspar dissolution rates were calculated for  $E_a$  values of 35, 49, and 65 kJ/mol. Line A represents the rate derived by simply taking the total observed alteration and dividing by 12.8 million years. The range used in the NFC model, and the point corresponding to the rate and  $E_a$  values used in the THC seepage model, are also plotted. The NFC model range for the ambient feldspar dissolution rate bounds the range of values calculated with the different possible thermal histories for the TSw tuff. For the THC seepage model values to conform with this analysis, either the feldspar dissolution rate or  $E_a$  must be much smaller.

There are two assumptions in these calculations. First, it is assumed that the same ambient alteration rate applies throughout time. This is not likely to be correct; in general, silicate dissolution rates are observed to decrease greatly with age in natural systems. However, the net effect of having a faster rate in the past is that the present-day dissolution rate would have to be even slower. Second, it is assumed that the feldspar dissolution rates at any given time are mostly a function of temperature and not of water composition; that is, there is no feedback to reduce the rate of feldspar alteration relative to that predicted using the Arrhenius relationship.

This is a reasonable assumption because precipitation of clays, zeolites, and even albite and microcline, keeps water compositions from approaching equilibrium with volcanic, mixed-composition feldspars. Hence, a far-from-equilibrium rate will be maintained. This argument is presented in more detail in *Engineered Barrier System: Physical and Chemical Environment* (SNL 2007a, Section 6.3.2.4.2).



NOTE: The preceding paragraphs discuss the relationship for lines A to E.

Figure 10. Plot Showing the Relationship between Calculated Ambient Feldspar Dissolution Rates and Activation Energy for Different Possible Thermal Histories (A through E)

## 1.5 REFERENCE TO THE THC SEEPAGE MODEL IN THE SEIS

The final paragraph in the RAI addresses a statement in the SEIS, which attributes a small decrease in dose, relative to that predicted previously with the THC seepage model in the 2001 FEIS, to implementation of the newer NFC model. The RAI also notes that this difference is not discussed in SAR 2.3.5.3.3.4. This difference is discussed in the SEIS but not in the SAR because the objective of the SEIS is to place current TSPA results into context with respect to the FEIS, and the dose calculations presented in the FEIS are based on a previous TSPA model. Since 2001, the TSPA model and many of the supporting process models, including the THC seepage model, have undergone revision. The current THC seepage model differs from the earlier version used in the FEIS in the following ways:

- Different starting waters are used (and four initial waters are used instead of five).
- Two thermal histories, representing repository center and edge conditions, are implemented instead of just one representing the repository center.
- An error in the implementation of transport equations in TOUGHREACT was found and corrected.

- A different mineral assemblage is now used—specifically, the current version of the THC seepage model implements an approach similar to that in the NFC model, using a single mixed alkali feldspar that can only undergo dissolution, instead of separate Na- and K-feldspar end-members that can reach equilibrium with the pore waters. Thermodynamic data for some minerals, used as fitting parameters to stabilize simulations of ambient conditions, have also changed.
- Silicate dissolution rates are decreased by a factor of 100 to 10,000. The previous model used laboratory-based rates, while the current model decreases those values to be more consistent with literature-reported field-based rates.
- A new suite of salt minerals is used in the normative salt precipitation routine that is implemented when pore-water dryout occurs.

Because of the scope of these changes in the current THC seepage model (SAR Section 2.3.5.2.3 and SNL 2007c) relative to the one discussed in the FEIS, and because the purpose of the THC seepage model has changed as discussed below, a detailed comparison in the SAR is not warranted.

The previous THC seepage model was implemented in the TSPA for the FEIS, using an abstraction that determined seepage compositions for all waste packages, using only simulations representing the hottest waste package locations. Later revision of the THC seepage model (SNL 2007c, Section 8.2) compared simulations for repository center and edge thermal conditions and showed that chemical conditions, such as the  $\text{Ca}^{2+}$  concentration, may be significantly different at cooler locations such as the repository edge. This led to the understanding that chemical conditions cannot generally be represented by extrapolation or interpolation of simulations for different locations, using differences in the local thermal-hydrologic responses. In addition, sensitivity studies were performed using the THC seepage model to examine seepage chemistry for hydrologic conditions when seepage is likely to occur (SAR Section 2.3.5.2.3). These studies showed that seepage is likely to be dilute, and that the accumulation of soluble salts in the host rock is limited.

Experience with the THC seepage model through successive revisions and sensitivity analyses indicated the need for an approach to modeling seepage chemistry for the TSPA that directly uses the local variations in temperature and percolation flux histories, that applies to hydrologic conditions for which seepage is likely to occur, and can be readily abstracted to incorporate the effects of these variations into the TSPA model. The NFC model was developed in response to this need. The purpose of the THC seepage model thereby changed from an abstraction for use in the TSPA for the FEIS, to its later use for FEP screening to support the TSPA. The SEIS (Table 5-1) identifies this change, acknowledging the improvement in approach and associating it qualitatively with a small decrease in dose response.

## 1.6 SUMMARY

In this RAI response, the integration of the NFC model with the seepage evaporation abstraction in the TSPA is described, and TSPA model results for the seepage evaporation abstraction are presented. The range of seepage water compositions generated by the TSPA model is strongly influenced by the treatment of uncertainty and variability in the contributing submodels. Whereas pore-water compositions from core samples collected during site characterization are not equivalent to equilibrated compositions on the waste package surface calculated by the TSPA model, they can be compared after in-drift temperatures have returned to ambient, and the pore-water compositions are shown to be generally bounded by the calculated results.

The RAI suggests that the THC seepage model represents an alternative conceptual model to NFC model. This response shows that the THC seepage model is not amenable to incorporating key parameter uncertainty and variability that is needed for the TSPA model. The THC seepage model is used primarily for evaluating the consequences of THC processes in support of FEP screening. The FEPs for which the THC model is used mainly deal with the effects of dryout and re-dissolution of salts around the drift on seepage chemistry, the effects of mineral precipitation on hydrologic properties of the host rock, and the effects of near-field chemical processes on radionuclide transport. It is not necessary for the THC seepage model to incorporate wide ranges of parameter uncertainty and variability to support these FEP screening justifications. A few representative conditions are examined, comprising a much smaller set of conditions than what is used in the TSPA-LA model to represent seepage composition.

The RAI suggests that the ambient feldspar dissolution rate and activation energy for feldspar dissolution implemented by the THC seepage model may represent an alternative conceptual model as well. The analysis presented in this response shows that parameterization used in the NFC model is appropriate, when the thermal history of the TSw tuff is considered. The slight over-prediction of feldspar dissolution by the THC seepage model during the thermal pulse has little effect on the evaluation of thermally driven coupled processes for FEPS screening decisions because the rate is still slow, and the thermal pulse is short.

## 2. COMMITMENTS TO NRC

None.

## 3. DESCRIPTION OF PROPOSED LA CHANGE

None.

#### 4. REFERENCES

SNL (Sandia National Laboratories) 2007a. *Engineered Barrier System: Physical and Chemical Environment*. ANL-EBS-MD-000033 REV 06. Las Vegas, Nevada: Sandia National Laboratories. ACC: DOC.20070907.0003; LLR.20080328.0031.

SNL 2007b. *In-Drift Precipitates/Salts Model*. ANL-EBS-MD-000045 REV 03. Las Vegas, Nevada: Sandia National Laboratories. ACC: DOC.20070306.0037; LLR.20080401.0242; DOC.20080707.0001.

SNL 2007c. *Drift-Scale THC Seepage Model*. MDL-NBS-HS-000001 REV 05. Las Vegas, Nevada: Sandia National Laboratories. ACC: DOC.20071010.0004; LLR.20080408.0266.

SNL 2008a. *Multiscale Thermohydrologic Model*. ANL-EBS-MD-000049 REV 03. Las Vegas, Nevada: Sandia National Laboratories. ACC: DOC.20080201.0003; LLR.20080403.0162; LLR.20080617.0077.

SNL 2008b. *Total System Performance Assessment Model /Analysis for the License Application*. MDL-WIS-PA-000005 REV 00 AD 01. Las Vegas, Nevada: Sandia National Laboratories. ACC: DOC.20080312.0001; LLR.20080414.0037; LLR.20080507.0002; LLR.20080522.0113; DOC.20080724.0005.

**RAI: Volume 3, Chapter 2.2.1.3.3, First Set, Number 6:**

The NFC model assumes chemical equilibrium between fracture and matrix waters. Fast flow-path fracture flow may cause chemical disequilibrium between fracture and matrix waters; thus the NFC model may not adequately represent the potential range of seepage water composition. Provide additional technical bases supporting the assumption that fracture and matrix waters are in chemical equilibrium. Demonstrate that seepage water compositions calculated using the NFC model adequately represent the potential range of seepage water chemistry.

**Basis:** In SAR Section 2.3.5, DOE used two lines of evidence to support the assumption of chemical equilibrium between matrix and fracture waters: (i) strontium and uranium isotope data and (ii) flow and transport modeling using the FEHM code. However, the isotope data only demonstrate that the fracture-matrix interactions are rapid relative to the precipitation of fracture-coating minerals, but do not demonstrate that the mineral precipitation is fast relative to downward transport through the fractures. Further, the FEHM code is a particle-tracking, finite element, heat and mass transfer code. It is not clear how the results from a particle-tracking model that uses a diffusion coefficient can be used to demonstrate chemical equilibrium between fracture and matrix pore waters.

Further, field observations of perched and matrix pore waters from the base of the TSw (boreholes SD-7, SD-9, NRG-7a, and UZ-14) suggest that fracture and matrix waters are in chemical disequilibrium.

**1. RESPONSE**

The near-field chemistry (NFC) model implements plug-flow in calculating water-rock interaction, as discussed in response to RAI: 3.2.2.1.3.3-007, hence it may appear that the approach assumes chemical equilibrium of fracture and matrix waters. However, the model incorporates an effective residence time based on simulations of dual-permeability (DKM) transport, to limit the extent of fracture-matrix interaction consistent with the active fracture model (AFM). The effective residence time controls a modified plug-flow type calculation that approximates DKM transport, and calculates water compositions that do not represent chemical equilibrium between fracture and matrix waters.

The effective residence time approximation in the NFC model represents the effects from percolation flux and fast pathways on the extent of water-rock interaction, and thus the influence on composition of potential seepage waters. The effective residence time is defined as the breakthrough time calculated using numerical, dual-permeability transport simulations that allow for disequilibrium between fracture and matrix waters. It approximates the minimum time that the solutes in fracture water have resided in the matrix porosity along the flow path to the repository. For the NFC model, the effective residence time is converted algebraically to the percolation flux that travels through a 200-m column of the host rock as plug-flow in the same time. Then, the corresponding average velocity (pore velocity) of this plug-flow is used to

calculate the extent of water–rock interaction as water traverses the changing temperature field above the repository. In this way, the extent of water–rock interaction (directly related to effective residence time) has a non-linear dependence on percolation flux, and the NFC model adequately represents the range of chemistry for potential seepage water.

## 1.1 SPECIES EXCHANGED BETWEEN FRACTURES AND MATRIX

In the conceptual basis for the NFC model, matrix and fracture waters are not necessarily in chemical equilibrium, i.e., the concentration of a given solute, such as  $K^+$ ,  $Na^+$ , or  $Ca^{2+}$ , may differ in fracture and matrix waters. The two rate-limited processes that control the similarity of matrix and fracture water compositions are feldspar dissolution, and fracture-matrix solute transfer by diffusion and advection. Both are represented in the NFC model: rate-limited feldspar dissolution is directly implemented using an Arrhenius rate equation, and limited fracture-matrix interaction is represented using effective residence time from numerical transport simulations. Other processes, including calcite and amorphous silica dissolution and secondary mineral precipitation, are much faster and are treated as local equilibria.

At low percolation flux values (i.e., present-day climate) the fracture and matrix waters will be close to chemical equilibrium with each other, as demonstrated from interpretation of strontium isotopes in recent fracture-lining calcite (SAR Section 2.3.5.3.2.2.1). This is part of the basis for the choice of matrix pore-water compositions, to represent inflowing fracture waters in the NFC model (see response to RAI: 3.2.2.1.3.3-001, which describes the technical bases for the range of pore-water compositions used to represent the natural system).

As the temperature of the host rock increases during repository heating, water–rock interaction in the matrix will increase, and the matrix pore-water composition will change. The extent of fracture-matrix interaction is inversely related to percolation flux and will determine the influence on fracture water composition. For much greater percolation fluxes that may occur in future climate states, chemical disequilibrium between fracture and matrix water compositions may occur, but the use of a single residence time calibrated to numerical simulations of fracture-matrix interaction is an appropriate way to represent the influence on fracture water composition (see response to RAI: 3.2.2.1.3.3-007, which describes the technical bases for solute residence times used in the NFC model). Local equilibrium with calcite, amorphous silica, and secondary precipitates is maintained, but fracture waters are influenced to an extent that is represented by the duration of water–rock interaction, controlled by the rate limiting processes described above.

The foregoing conceptual description of the effective residence time feature of the NFC model differs from discussion in the SAR (particularly Sections 2.3.5.3.2.2 and 2.3.5.3.3.2), which emphasizes fracture-matrix chemical equilibrium. The FEHM simulations performed originally to support the NFC model indicated near-equilibrium between fractures and matrix. However, results reported in response to RAI: 3.2.2.1.3.3-007 using T2R3D to correct fracture parameterization errors, and to include the AFM in the determination of flow fields, show that chemical disequilibrium between fractures and matrix becomes more important as percolation flux increases above 10 mm/yr. The NFC model formulation accommodates such disequilibrium

using effective residence time, and the NFC model plug-flow velocity is calibrated to the revised transport simulations in the response to RAI: 3.2.2.1.3.3-007.

## 1.2 SIMULATIONS OF FRACTURE-MATRIX INTERACTION

The initial transport results using FEHM V. 2.24 (2006) produced steep breakthrough curves suggesting near-equilibrium between fracture and matrix waters for percolation flux of up to 100 mm/yr. The response to RAI: 3.2.2.1.3.3-007 shows that a broader distribution of residence times (greater “tailing” of breakthrough curves) is obtained when using T2R3D as described in that response. However, the mean residence time can be used to represent the time available for water–rock interaction to influence solute chemistry. Water arriving at the repository can be considered to have a distribution of residence times corresponding to the tails of the breakthrough curves calculated by releasing tracer as an instantaneous pulse. For continuous tracer release (representing *in situ* water–rock interaction) the breakthrough curves can be mathematically integrated to represent the water composition arriving at the repository. The extent of feldspar dissolution is proportional to residence time, so the mean residence time can be used to compute the average quantity of feldspar dissolved in water arriving at the repository for nearly isothermal, steady-state conditions. Note, however, that feldspar dissolution rates are temperature dependent, and the host-rock temperature changes because of repository heating, so it is not appropriate to use a residence time that is long relative to the duration of the repository thermal pulse. The difference between mean and median residence times increases for higher percolation flux, for example, the 100 mm/yr case evaluated in the response to RAI: 3.2.2.1.3.3-007 has a median residence time of 19 years and a mean residence time of 312 years (Figure 1 of that response). Therefore, shorter median residence times are used in the analyses documented in the response to RAI: 3.2.2.1.3.3-007 rather than mean residence times to avoid overestimating the degree of feldspar dissolution in percolating waters.

## 1.3 COMPARISON OF PERCHED AND PORE-WATER COMPOSITIONS

Inspection of available perched water and pore-water analyses for boreholes SD-7, SD-9, NRG-7/7a, and UZ-14 (Table 1) found no instances of co-located samples from which a direct comparison can be made of matrix pore-water composition within perched zones.

Perched water is found only below the proposed repository level, as perched water bodies adjacent to subunits within the Calico Hills Formation or situated on the basal vitrophyre of the Topopah Spring Tuff. Perched waters are sodium-bicarbonate type, with especially low concentrations of chloride compared to matrix pore water (Table 1). Perched waters have apparent radiocarbon ages on the order of 10 kyr, which is generally older than radiocarbon ages determined for water in the overlying rock. Perched waters have  $^{234}\text{U}/^{238}\text{U}$  activity ratios similar to fracture minerals in the overlying rock, indicating transport by fracture-flow (SAR Section 2.3.2.3.4.3).

Pore waters from core samples originating above and below perched water bodies have chemical characteristics (particularly the range of chloride concentrations) that are more similar to one another than to perched waters (Figure 1). The chloride content of perched waters is so low that it overlaps that of precipitation. Given the presence of old chloride-containing soils, such low

chloride concentrations cannot be preserved by net infiltration that occurs over most of the Yucca Mountain site. This indicates that the perched waters were recharged during colder climates, along isolated, fast pathways. An alternative explanation is that perched waters, being similar to saturated zone water, may have originated from higher water tables and/or lateral flow from the north where the groundwater table is at a higher elevation. For either explanation of origin, pore water and perched water have distinctly different geochemical evolution and have undergone different degrees of evaporation, water-rock interaction, or both (SAR Section 2.3.2.3.4.1). Thus comparisons between perched and pore-water compositions cannot be used to evaluate model predictions of fracture-matrix interaction in the unsaturated host rock.

Table 1. Representative Compositional Analyses for Perched Water and Nearby Pore-Water Samples from Boreholes SD-7, SD-9, NRG-7/7a, and UZ-14

Sample ID	Type	Depth (m)	pH	Conductivity (µS/cm)	Na (mg/L)	K (mg/L)	Mg (mg/L)	Ca (mg/L)	SiO <sub>2</sub> (mg/L)	HCO <sub>3</sub> (mg/L)	CO <sub>3</sub> (mg/L)	Cl (mg/L)	SO <sub>4</sub> (mg/L)	NO <sub>3</sub> (mg/L)	Br (mg/L)
NRG-7A/1483.5-1483.8/CHn/BT	Pore	452.2	7.9	580	94.0		0.6	61.0	48.6	323.0	0.0	33.1	24.4	16.7	0.1
NRG-7A/1492.7-1493.1CHn/BT	Pore	455.0	7.9	580	74.7		0.3	30.6	71.5	104.0	34.0	39.0	23.0	18.0	0.0
NRG-7A/1498.6-1498.9/CHn/BT	Pore	456.8	7.5	500	73.2		0.5	28.7	83.0	156.0	0.0	50.0	18.0	17.0	0.0
NRG-7A	Perched	458.8	8.7	224	42.0	6.8	0.0	3.0	9.0	114.0	0.0	7.0	4.0	1.0	0.0
SD-7/1558.4-1558.6/CHn	Pore	475.0	7.2	390	43.0		0.9	39.0	69.3	171.0	0.0	25.1	14.9	9.0	0.1
SD-7(3/16)	Perched	485.9	8.1	239	45.0	5.3	0.1	13.0	57.0	128.0	0.0	4.1	9.1	34.0	0.0
SD-7(3/17)	Perched	485.9	8.2	265	46.0	5.5	0.0	13.0	51.0	130.0	0.0	4.1	8.6	23.0	0.0
SD-7(3/20)	Perched	485.9	8.0	265	46.0	5.4	0.0	13.0	55.0	127.0	0.0	4.1	8.5	13.0	0.0
SD-7(3/21)	Perched	485.9	8.2	259	45.0	5.5	0.0	14.0	56.0	128.0	0.0	4.1	10.0	13.0	0.0
SD-7/1600.1-1600.3/CHn	Pore	487.7	7.6	380	59.0		0.6	23.0	66.7	150.0	0.0	31.0	12.0	5.7	0.0
SD-9/1452.6-1452.8/TSw	Pore	442.8	7.3	530	112.0		0.0	6.9	62.5	256.0	0.0	15.7	12.3	10.6	0.1
SD-9/TS	Perched	453.1	8.6	445	98.0	9.8	0.2	2.9	64.0	197.0	10.0	5.6	28.0	3.3	0.0
SD-9/1535.2-1535.4/CHn	Pore	468.0	7.4	530	112.0	7.0	0.1	0.8	54.9	226.0	0.0	15.6	15.5	10.6	0.9
SD-9/1619.9-1661.4/CHn	Pore	500.1	8.3	610	136.6	4.0	0.0	0.4	55.6	232.0	12.0	50.2	18.3	9.0	0.1
SD-9/1661.1-1661.3/CHn	Pore	506.3	8.1	660	164.0		0.0	0.7	48.8	317.0	0.0	42.0	18.9	8.2	0.1
UZ-14/1258.5-1258.8/up1	Pore	383.6			67.0		3.7	43.0	35.0	170.0		88.0	19.0	16.0	0.0
UZ-14-PT-2	Perched	387.9			35.0	3.3	2.4	30.0	26.0	144.0	0.0	7.0	23.0	15.0	0.1
UZ-14-PT-4	Perched	387.9			34.0	1.8	2.1	27.0	32.0	142.0	0.0	6.7	14.0	15.0	0.1
UZ-14/1277.4-1277.7/up1	Pore	389.4			49.0		4.5	62.0	44.0	170		87.0	45.0	17.0	0.0
UZ-14/1277.7-1278.0/up1	Pore	389.5			45.0		5.1	74.0	38.0	170		130.0	38.0	15.0	0.0
UZ-14/1409.4-1409.8/up1	Pore	429.7	7.8	720	88.0		0.7	30.0	57.0	160.0	0.0	75.0	106.0	5.0	0.0
UZ-14/1419.5-1419.8/up1	Pore	432.7	8.3	410	68.0		0.6	20.0	60.0	166.0	0.0	24.0	21.0	6.0	0.0

NOTE: Constituents not tabulated were not analyzed.

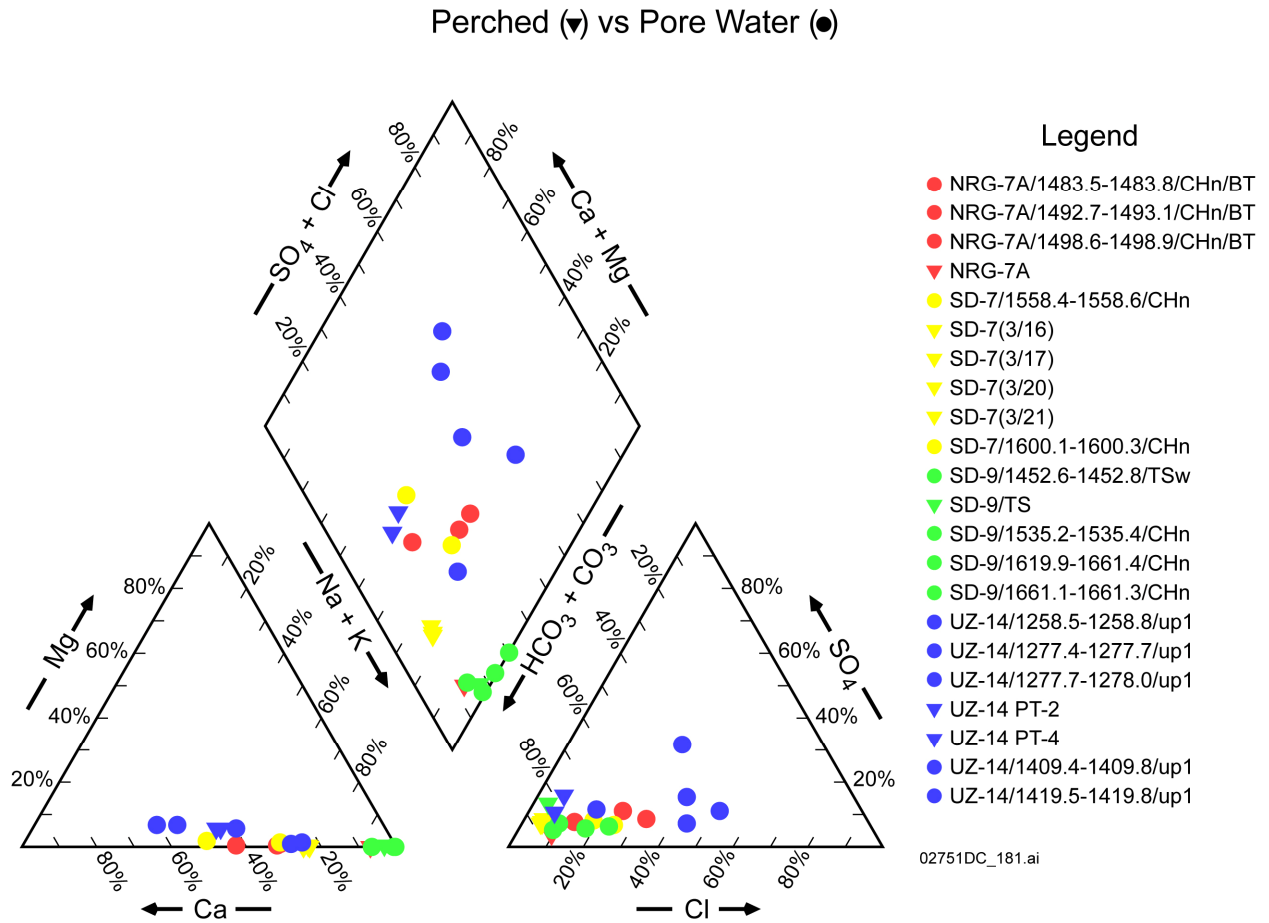


Figure 1. Piper Plot for Compositions of Perched Water and Pore-Water Samples from Table 1

## **1.4 SUMMARY**

The NFC model implements plug-flow in calculating water–rock interaction, but does so in a way that uses solute residence time to approximate DKM transport, and does not require chemical equilibrium between fracture and matrix waters. The effective residence time approximation in the NFC model represents the effects from percolation flux and fast pathways on the extent of water–rock interaction and the composition of potential seepage waters. This conceptual description differs from the discussion in SAR Section 2.3.5.3, which emphasizes fracture-matrix chemical equilibrium. The FEHM simulations performed originally to support the NFC model indicated near-equilibrium; however, results reported in the response to RAI: 3.2.2.1.3.3-007 show that chemical disequilibrium between fractures and matrix becomes more important as percolation flux increases above 10 mm/yr. The NFC model formulation accommodates such disequilibrium using the effective residence time approximation.

The effective residence time is defined as the breakthrough time from numerical, dual-permeability simulations of solute transport (see the response to RAI: 3.2.2.1.3.3-007), which allow disequilibrium between fracture and matrix waters, and which are consistent in concept and parameterization with the unsaturated zone transport model. The two rate processes that control the chemical evolution of fracture water—matrix diffusion and feldspar dissolution—are represented using effective residence time and an Arrhenius rate law. The effective residence time thus captures the effects from fracture-matrix disequilibrium and, along with other factors described in the response to RAI: 3.2.2.1.3.3-002, allows for a representative range of seepage water chemistries to be computed in the TSPA.

## **2. COMMITMENTS TO NRC**

Captured under Section 2 of RAI: 3.2.2.1.3.3-007.

## **3. DESCRIPTION OF PROPOSED LA CHANGE**

Captured under Section 2 of RAI: 3.2.2.1.3.3-007.

## **4. REFERENCE**

FEHM V. 2.24. 2006. 5.9/2.4.21/WINXP/WIN 2000. STN: 10086-2.24-00.